A status report on the NRC sealed water calorimeter

Seuntjens, J. P.; Ross, C. K.; Klassen, N.; Shortt, K. R.

https://doi.org/10.4224/8899774

A Status Report on the NRC Sealed Water Calorimeter

J. P. Seuntjens, C. K. Ross, N. V. Klassen and K. R. Shortt

March, 1999

PIRS-0584

Ionizing Radiation Standards
Institute for National Measurement Standards
National Research Council
Ottawa, Ontario K1A 0R6 Canada

(A preliminary draft of this report, dated April, 1997, was distributed to a few individuals. This is the final version.)

Telephone: 613-993-9352
Fax: 613-952-9865
E-mail: jan.seuntjens@nrc.ca

Abstract

One technique for establishing the absorbed dose to water under reference conditions is calorimetry. The Ionizing Radiation Standards Group at NRC has focused its efforts on water calorimetry and, in previous work, used a small calorimeter containing stirred water to study the heat defect of various aqueous systems. This same calorimeter, combined with high-precision Fricke dosimetry, was also used to establish the absorbed dose at a point in a large water phantom.

More recently, a large water calorimeter, capable of giving directly the dose at a point, has been constructed. The water quality at the measurement point is controlled by isolating a small volume of water within a sealed glass vessel. An extensive set of measurements using this calorimeter has now been completed using ^{60}Co γ-rays and 20 MV x-rays. This report describes the main design features of the calorimeter and summarizes the results of the measurements.

For the optimum run time (about 120 s) the sample standard deviation is about 0.8% for an absorbed dose of about 3 Gy. This leads to a standard uncertainty on the mean of about 0.3% for a series of 10 runs. The absorbed dose measured when operating the calorimeter at 4°C is 0.7% lower than the value obtained when operating at 22°C. Calculations indicate that this discrepancy is likely due to convective heat transfer at 22°C.

Contents

List of Figures

List of Tables

1 Introduction

Radiation therapy requires that the absorbed dose to the patient be known accurately. The first step in determining the dose to the patient is to determine the dose to water under well-defined reference conditions. One of the best techniques for establishing the absorbed dose absolutely is calorimetry and, for many years, graphite was considered the best material to use for building an absorbed dose calorimeter. The main features of various graphite calorimeters have been reviewed by Laughlin and Genna (1966) and Domen (1987), and graphite calorimeters continue to be used as absorbed dose standards (DuSautoy 1996; Guerra *et al* 1996; Chauvenet *et al* 1997). The principal disadvantage of graphite calorimetry is that a conversion process is necessary in order to convert from dose-to-graphite to dose-to-water.

Several years ago Domen (1980) showed that it was possible to construct and operate a large water calorimeter. However, results with early water calorimeters were disappointing in that the measured absorbed dose was several percent different from that obtained using conventional dosimetric techniques. It was soon recognized that the most likely reason for the discrepancy was due to a heat defect caused by radiation-induced chemical reactions in the water. Our group has devoted considerable effort to the study of the heat defect of aqueous systems (for a review of the literature, see Ross and Klassen (1996)) and we have identified several aqueous systems which are well suited for water calorimetry.

Until recently, all our work on water calorimetry has been carried out using a small water calorimeter in which the water was stirred (Ross *et al* 1984). This design was well suited to the study of the relative response of various aqueous systems. The small size eased the problem of keeping the calorimeter clean, and the small water volume (100 ml) permitted the water to be saturated quickly with various gas mixtures. By stirring the water, thermal equilibrium could be quickly established, thus allowing several aqueous systems to be studied in a short time.

On the negative side, a small calorimeter containing stirred water cannot be used for establishing directly the dose at a point in a large water phantom. We were able to overcome this limitation by using the small calorimeter to calibrate Fricke dosimeter solution in terms

of absorbed dose to water (Ross *et al* 1989). The calibrated Fricke solution was then used to establish the dose at a point in a large water phantom (Shortt *et al* 1993). The main technical challenge in determining the absorbed dose to the stirred water arises from the need to determine the heat transferred to the water from the irradiated glass. In addition, the effect of the vial walls on the Fricke response must be known (Ma *et al* 1993). A significant limitation of this approach is that it requires not only expertise in water calorimetry, but also in high-precision Fricke dosimetry.

Our studies of the heat defect of various aqueous systems showed that water quality must be carefully controlled. Using this knowledge, Domen (1994) constructed a large water calorimeter containing a smaller, sealed element which could be filled with a well-defined aqueous system. Because the temperature sensors were located within the sealed vessel, the temperature change was measured in water having a known heat defect. He referred to the calorimeter as a sealed water (SW) calorimeter. Domen showed that measurements with either N_2-saturated or H_2-saturated water gave results for ^{60}Co γ-rays which were in good agreement with the results obtained using graphite calorimetry.

Seuntjens *et al* (1993a), (1993b) constructed a calorimeter similar in design to that of Domen. They used it to measure the absorbed dose due to medium energy x-ray beams (Seuntjens *et al* 1993a), to study the heat defect of various aqueous systems (Seuntjens *et al* 1993b) and to measure the absorbed dose due to protons (Palmans *et al* 1996). For ease of construction, Seuntjens *et al* used Lucite rather than glass for the walls of the sealed vessel within the larger water volume. This led to some difficulties with reproducibility at low doses, presumably due to contamination of the water by the Lucite.

We have completed the construction of a calorimeter which combines the major design features of both the Domen and Seuntjens calorimeters. The calorimeter has passed various operational tests and has been used for measurements of the absorbed dose to water in a ^{60}Co γ-ray beam and a 20 MV x-ray beam.

In section 2 we describe the main features of the calorimeter, while in section 3 we outline how the calorimeter is used to establish the absorbed dose. Section 4 shows how the calorimeter responds to ^{60}Co γ-rays, while section 5 summarizes its response using different aqueous systems. Sections 6 and 7 describe the results of measurements of the absorbed

dose to water obtained using ^{60}Co γ-rays and 20 MV x-rays.

2 Calorimeter Design

For graphite calorimetry, the volume element in which the radiation-induced temperature rise is to be measured must be thermally isolated from the rest of the phantom. However, the thermal diffusivity of water is much smaller than that of graphite, and Domen (1980) showed that, under appropriate conditions, the temperature rise could be measured directly at a point in a large water phantom. Ignoring for the moment various correction factors, the dose to water, D_{w}, is given by

$$D_{\mathrm{w}} = c_{\mathrm{w}} \cdot \Delta T_{\mathrm{w}}, \tag{1}$$

where ΔT_{w} is the measured temperature increase and c_{w} is the specific heat capacity of water. At room temperature the specific heat capacity of water is approximately 4180 (J/kg)/K, so an absorbed dose of 1 Gy gives a temperature rise of only 0.2 mK.

The NRC SW calorimeter is based on the design developed by Seuntjens (1991) at the University of Gent, Belgium. In this section we summarize the construction details, the electronic circuitry and the measuring techniques for the NRC calorimeter. In addition, we identify various correction factors which are required for accurate absorbed dose determination. These include corrections for conductive heat transfer, for radiation-induced chemical reactions and for the effects of perturbations of the radiation field due to the presence of non-water materials. Each of these effects may influence the actual measured temperature increase, ΔT_{w}, and therefore the measured dose.

2.1 Overview of the Calorimeter

The main elements of the calorimeter are shown schematically in figure 1. Note that it is intended for use in radiation beams that are directed horizontally. The water is held in a Lucite tank, 30 cm on each side. The exterior walls of the tank are insulated with 5 cm thick Styrofoam. A magnetic stirrer for agitating the water is built into the bottom of the tank. The lid on the tank contains several holes through which calibrated platinum resistor probes

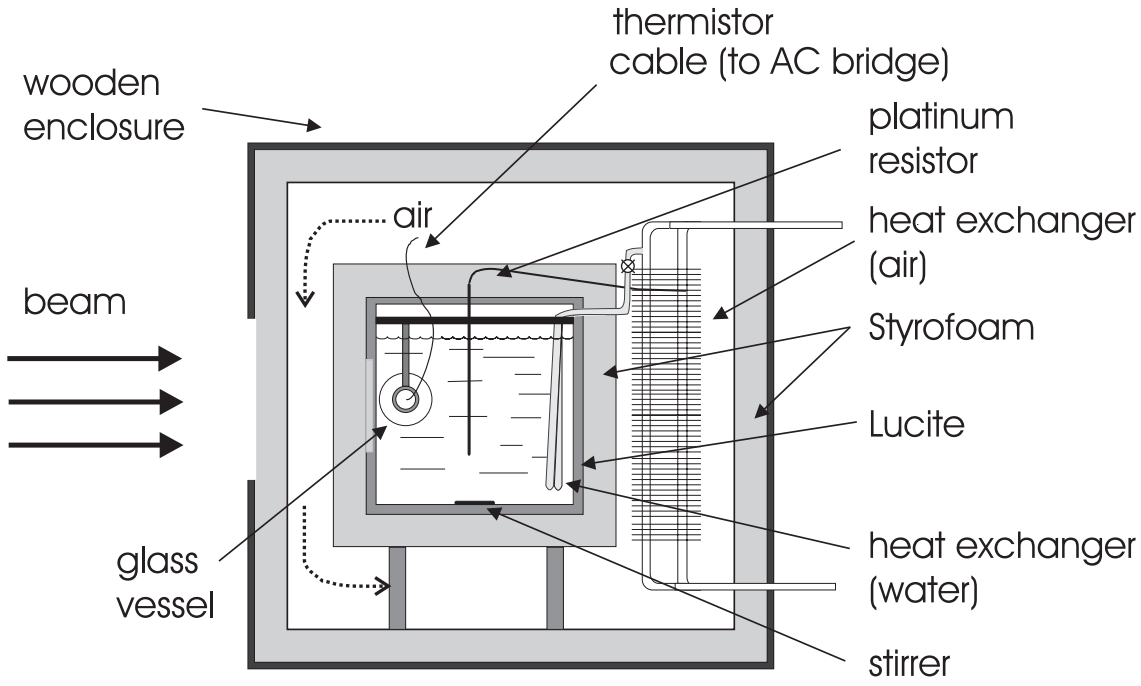

Figure 1: Side view of the sealed water calorimeter. The drawing is not to scale, but the sides of the outer box are approximately 85 cm long. The principal elements of the calorimeter are labelled on the drawing. Note that fluid is only allowed to flow through the heat exchanger in the water when a significant change in operating temperature is required.

are inserted to measure the water temperature. The lid also ensures a motion-free air space above the water surface. The window of the tank through which the radiation field enters is machined down to 3 mm over an area of 12 cm by 12 cm. The window is thermally isolated with a removable, 5 cm thick Styrofoam plate. The calorimeter phantom is enclosed in an insulated wooden box, 85 cm on each side, in which the temperature is stabilized using fans and a heat exchanger. The cooling fluid can also be made to pass through a heat exchanger in the water tank so as to accelerate the process of changing the operating temperature of the water in the calorimeter. The calorimeter is designed for operation at any temperature from 0°C to 25°C. It typically takes 3 to 4 hours to bring the temperature to 4°C when starting from room temperature. The bath controlling the temperature of the liquid in the heat exchangers is stable to ±0.1°C. An additional calibrated platinum resistor probe monitors the temperature of the air circulating around the calorimeter.

2.2 Glass Detection Vessel

The temperature increase due to irradiation is measured in the centre of a cylindrical glass vessel which is designed to isolate a small volume of high purity water from the water in the rest of the phantom. A typical detection vessel is shown in figures 2 and 3. It consists of a central cylindrical portion, about 75 mm long, which is attached to conical end pieces. Threaded fittings on the end pieces hold the thermistor probes in place. The vessel is mounted in the water tank on an adjustable slide so that its position along the beam axis can be varied.

The cylindrical portion of the first vessel we used was formed using glass blowing techniques. This approach led to considerable variation in the wall thickness (see figure 4), and the vessel was not perfectly round. Variation in the wall thickness lead to uncertainties in the wall correction factors, and lack of roundness makes it difficult to establish the probe position within the vessel. This vessel is referred to as #1, and it has an outside diameter of approximately 67 mm.

Later vessels have been formed by first grinding glass tubing to a wall thickness of 1 mm. Because precision grinding techniques are used, similar to those used for making lenses, the wall thickness is uniform and the vessels closely circular. The conical end pieces are attached

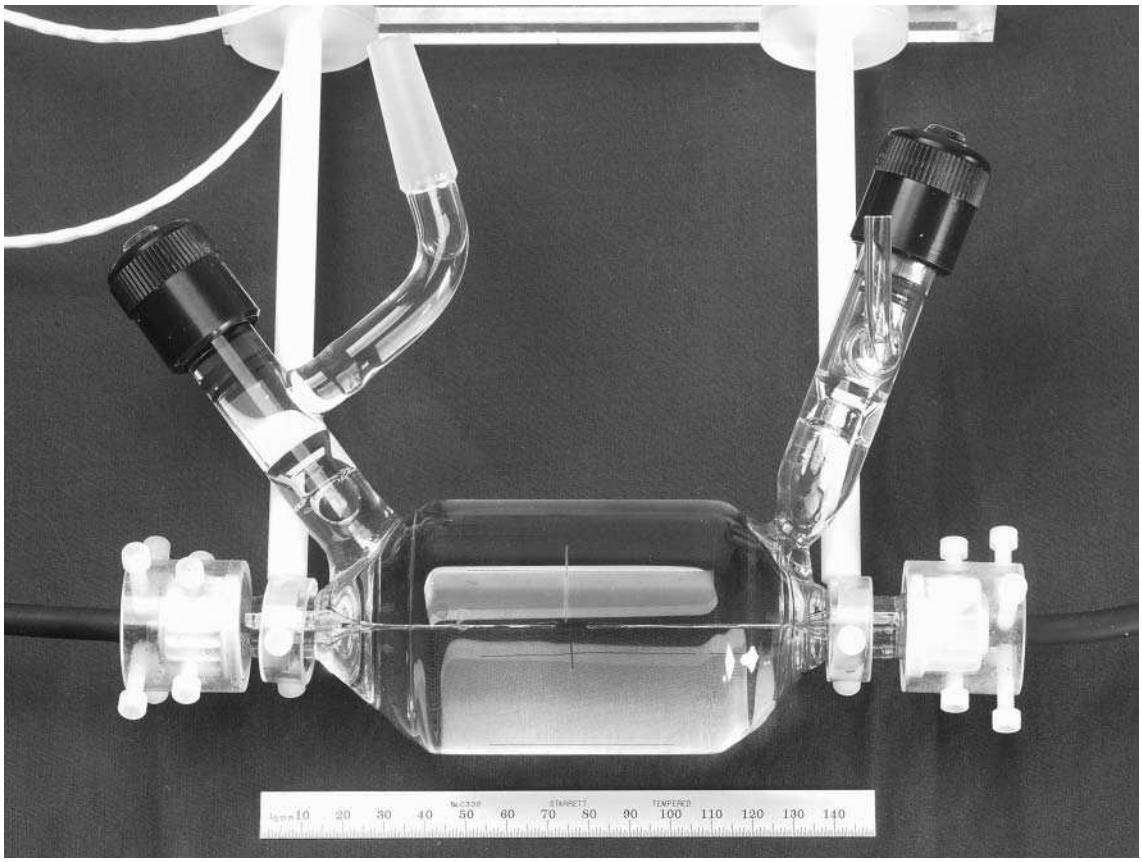

Figure 2: Glass detection vessel No. 3, with the thermistor probes aligned in the centre. The thick white line in the upper left of the photograph is part of the thermistor signal cable after it has emerged from the waterproof tubing.

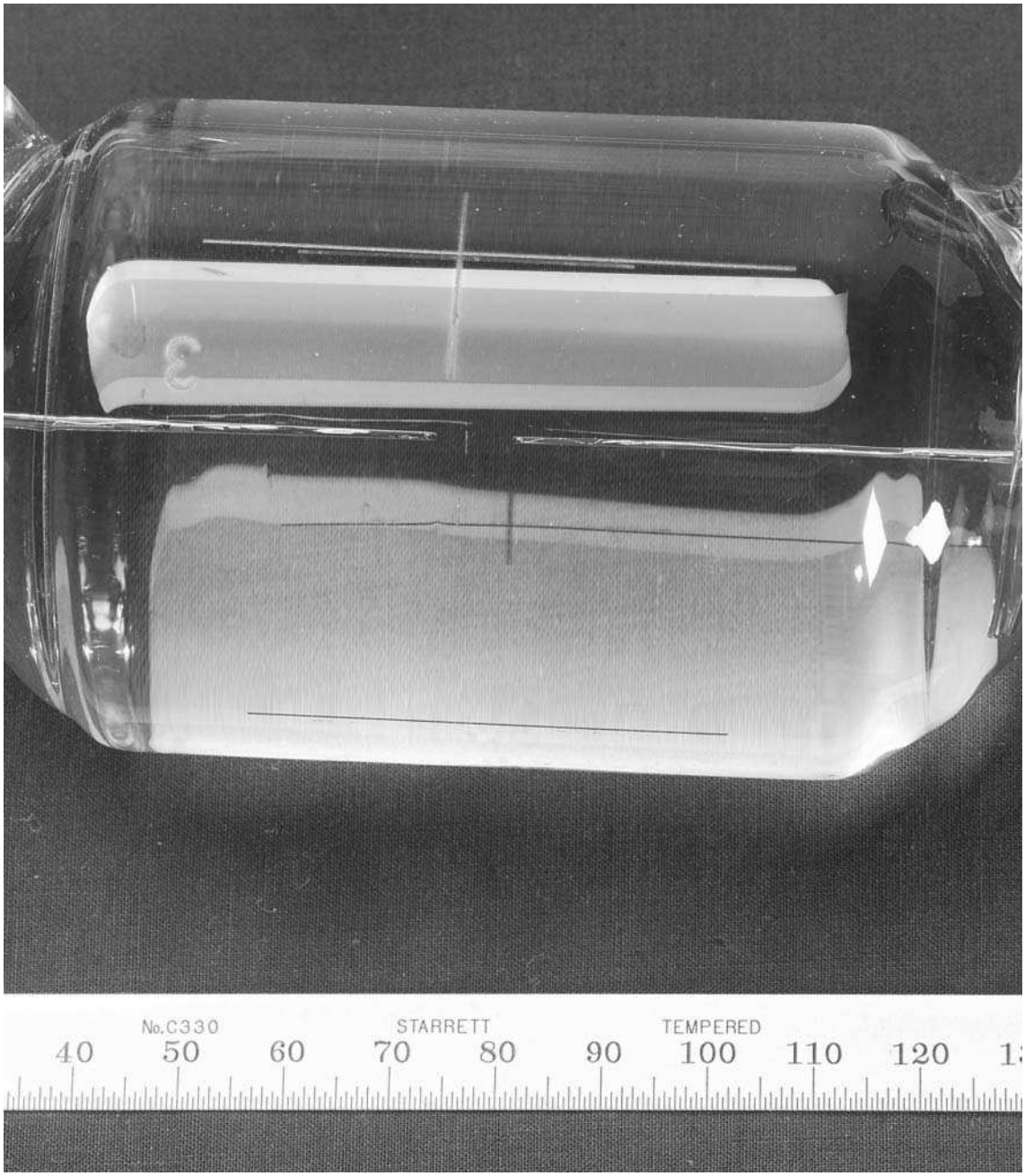

Figure 3: A close-up view of glass detection vessel No. 3, with the thermistor probes aligned in the centre. The alignment decals are visible on the glass wall.

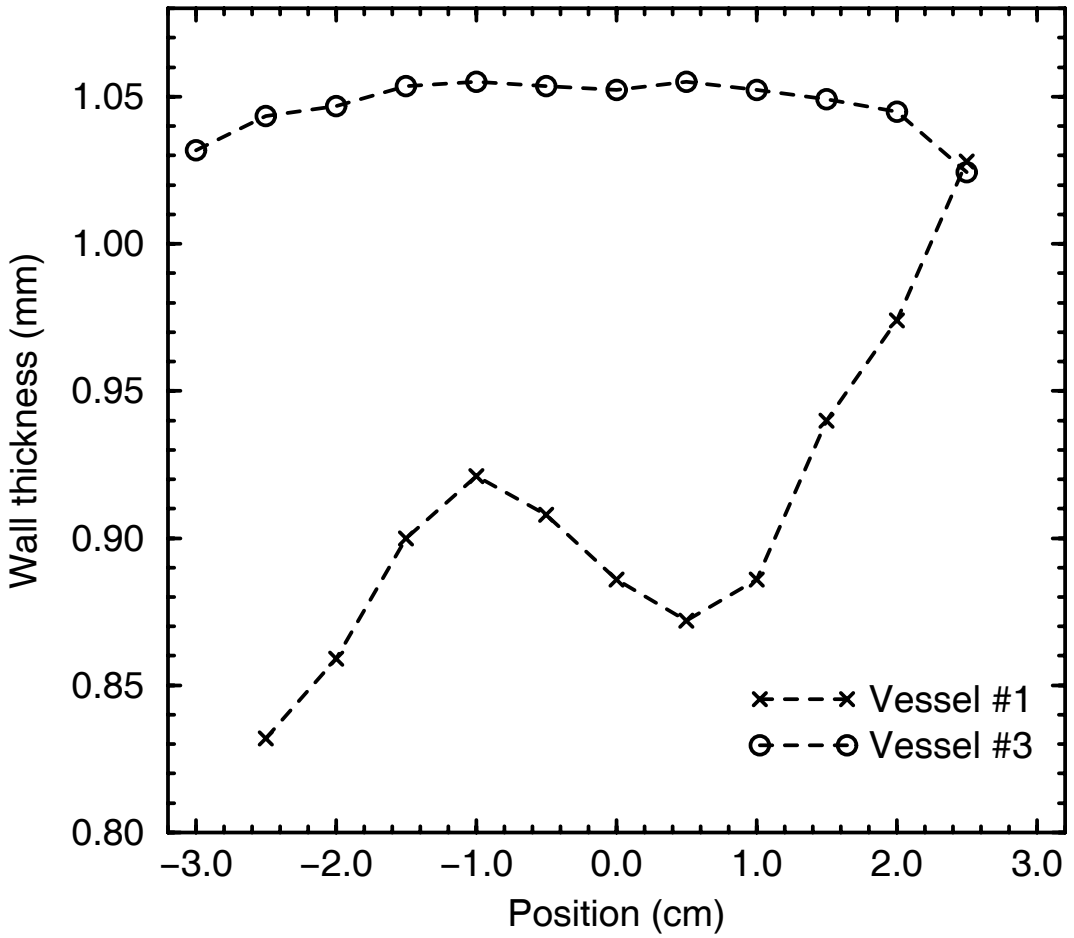

Figure 4: Variation of the vessel wall thickness along the length of the cylindrical portion. The measurements were done using a liquid displacement technique, and thus represent the average wall thickness at that position. Vessel #1 was formed using glass blowing techniques, while the cylindrical portion of vessel #3 was formed by grinding glass tubing to the required dimensions.

to the central cylindrical section using glass blowing techniques. The first vessel constructed in this way was labelled #3, and it has an outside diameter of 61.53 mm. Its wall thickness as a function of position is shown in figure 4.

Because the rate at which heat from the glass vessel is transferred to the measuring point depends strongly on the vessel diameter, it was decided to construct any additional vessels with a diameter close to that of vessel #1. Vessels #4 through #7 have a mean outside vessel diameter of approximately 67.56 mm, and the length of the cylindrical portion is about 90 mm. The variation of the diameter from vessel to vessel, and from point to point on each vessel, is shown in figure 5. The total variation in diameter is less than 0.1 mm. The variation in wall thickness from vessel to vessel and within each vessel is shown in figure 6. The maximum deviation from the nominal 1 mm thickness is 0.1 mm.

Before the ends are attached to the cylinders, an indexing machine is used to mark the circumference at 90° intervals. Ceramic decal lines are placed on each mark and fixed in place by annealing the cylinders at 560°C. These lines have a width of 0.4 mm and are used for aligning the probes within the vessel, and the vessel within the phantom.

A glass valve is attached to either end of the vessel to allow it to be filled, drained and bubbled with various gases. Upon sealing off the vessel, care is taken to be sure a small gas bubble is left behind. This bubble allows the water to expand and contract between 4°C and 22°C without breaking the vessel.

Temperature measurements in the vessel are performed using glass thermistor probes, the ends of which can be positioned at the centre of the vessel using a set of screws (see figure 2). Originally, the appropriate positioning of the probe ends with respect to lines on the outside of the vessel was done using a telescope. In a separate investigation we established that optical distortion did not affect the alignment by more than 0.2 mm. Since then, we have found that probe alignment can be done adequately by eye, certainly within ± 0.2 mm.

When preparing for measurements, the vessel is first filled with high purity water, and then bubbled for one to two hours with H_2, H_2 and O_2, N_2 or Ar gases, depending on the aqueous system to be used. Then the probe position is adjusted and the vessel is suspended in the water phantom. Calorimetric measurements can be started typically three hours later if the water in the tank is at operating temperature and the bubbling is done at room

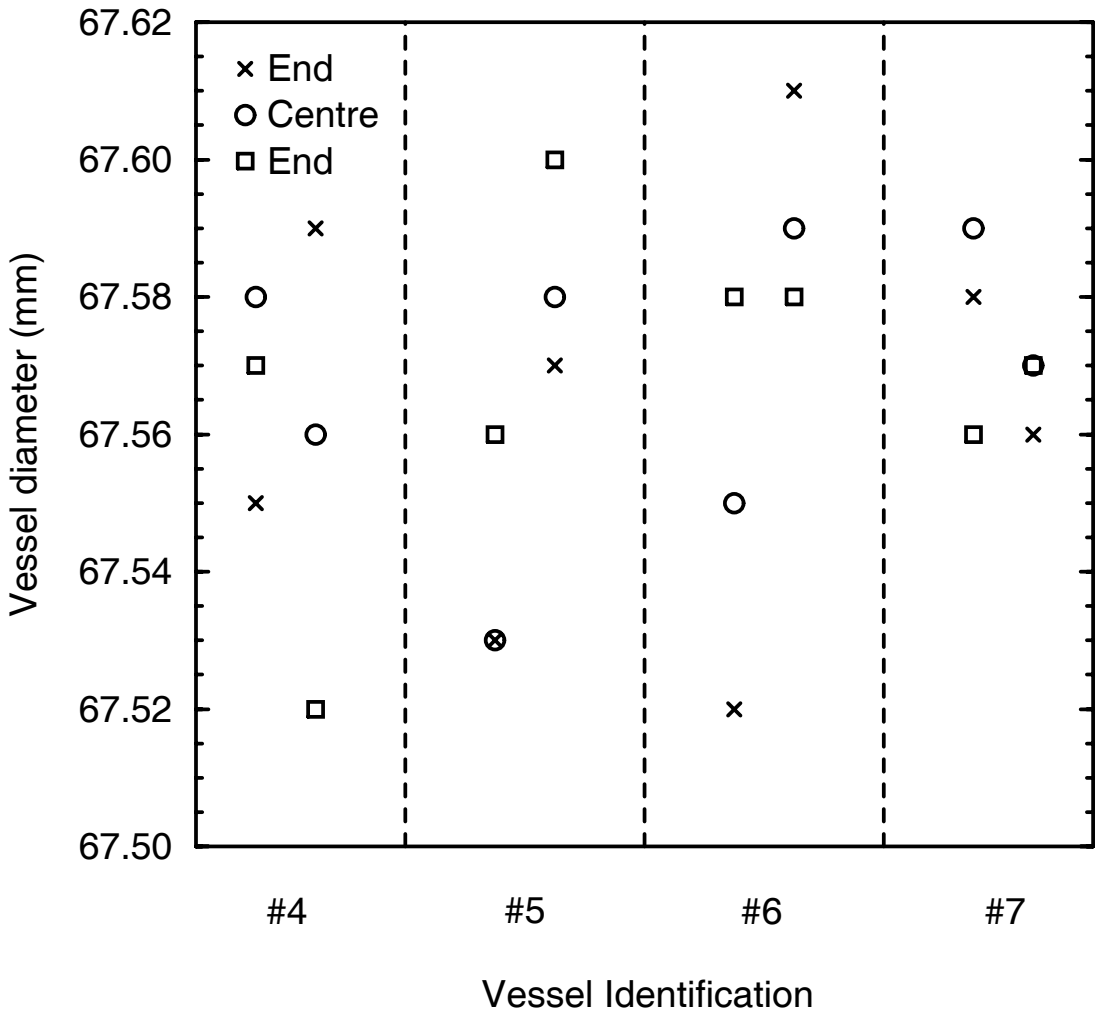

Figure 5: Variation of the vessel diameter from vessel to vessel and within each vessel. The three data points in each vertical column correspond to measurements in one plane passing through the axis of the cylinder. The second column associated with each vessel corresponds to measurements in a plane at 90° with respect to the first. The positions labelled "End" were approximately 20 mm from each end of the cylinder, or about 25 mm from the centre.

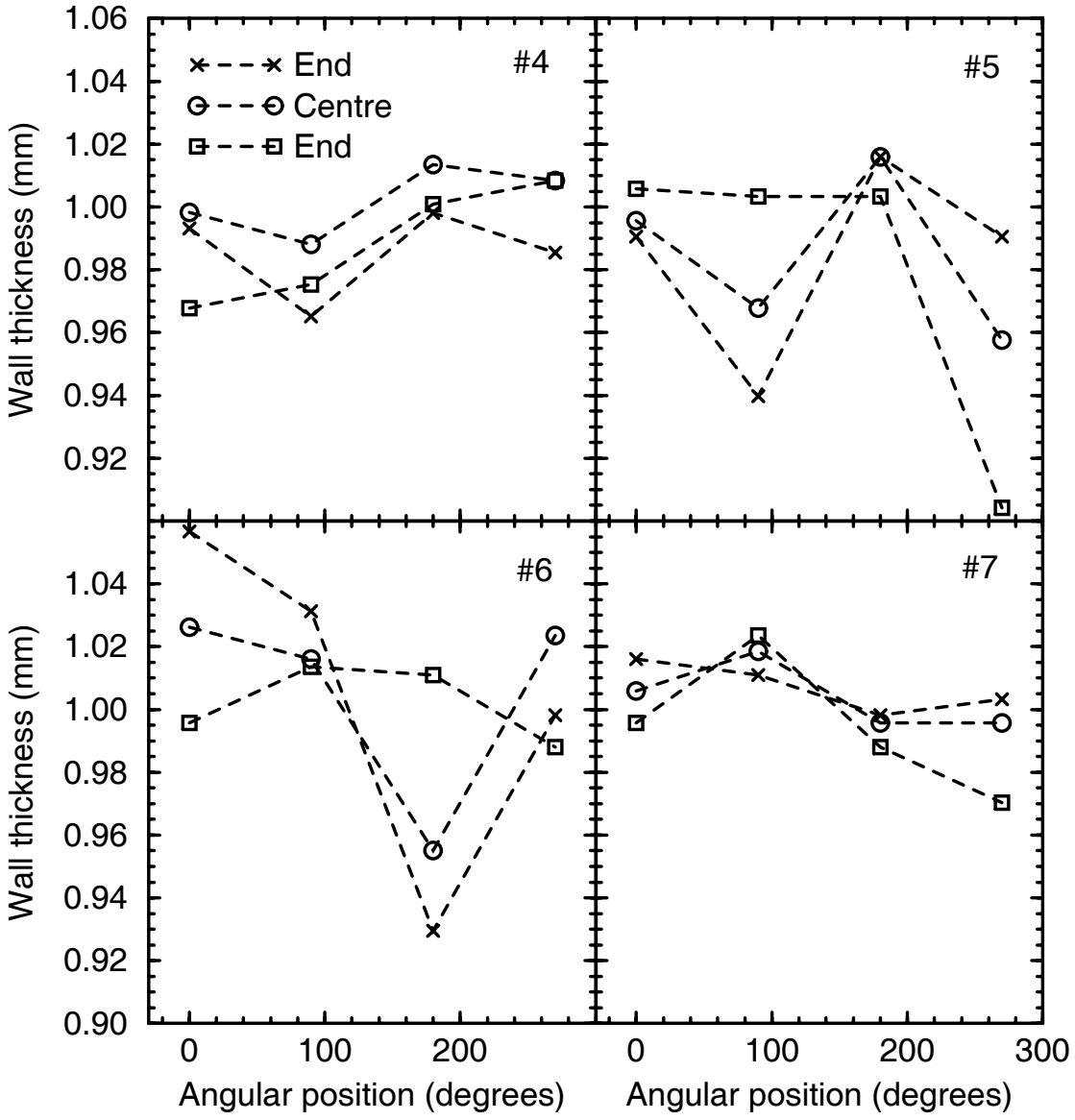

Figure 6: Variation of the vessel wall thickness from vessel to vessel and within each vessel. The positions labelled "End", "Centre" and "End" have the same meaning as in figure 5.

temperature.

All the results given in this report have been obtained using either vessel #1 or #3.

2.3 Thermistor Probes

Our procedure for constructing thermistor probes is somewhat different from that recommended by Domen (1994). We begin with Pyrex tubing having a diameter of 8 mm and a wall thickness of 1 mm. The tubing is heated and pulled down to an outside diameter of 0.5 to 0.6 mm over a length of 4 cm. The inside diameter is checked using 0.3 mm diameter wire. Probes of acceptable dimensions are then flame-sealed on the small end and tested for leaks using a helium leak detector. We estimate the thickness of the glass wall at the thermistor bead to be 0.06 mm to 0.11 mm. The 0.03 mm diameter wires of the Thermometrics thermistors (0.25 mm in diameter) are soldered to 0.1 mm diameter copper extension wires, and one wire of the pair is inserted into 0.2 mm diameter microtubing to avoid electrical shorts. The bead and lead assembly is then slid into the glass envelope. Using a piece of microtubing, UV-curable adhesive is injected into the end of the probe to glue the thermistor bead to the glass. A Delrin rod is fitted into the large end of the glass probe to act as a strain relief for the screened cable to which the 0.1 mm copper extension wires are soldered. Waterproofing is achieved by passing the signal cable through a latex rubber tube which is stretched over the end of the glass tubing to form a water-tight seal. The latex tube is sufficiently long that the open end is outside the water phantom. The details of the probe construction are shown in figure 7.

2.4 Electronics

DC bridge techniques were used by Domen (1994) for the NIST water calorimeter, while Seuntjens (1991) used an AC bridge. Either approach provides adequate sensitivity for absorbed dose calorimetry, although the noise performance of the AC approach is probably superior. Although all our previous work on calorimetry at NRC has used DC bridges, we have chosen to use an AC bridge with the new water calorimeter.

Figure 8 is a schematic diagram of the electronics used with the calorimeter. The plat-

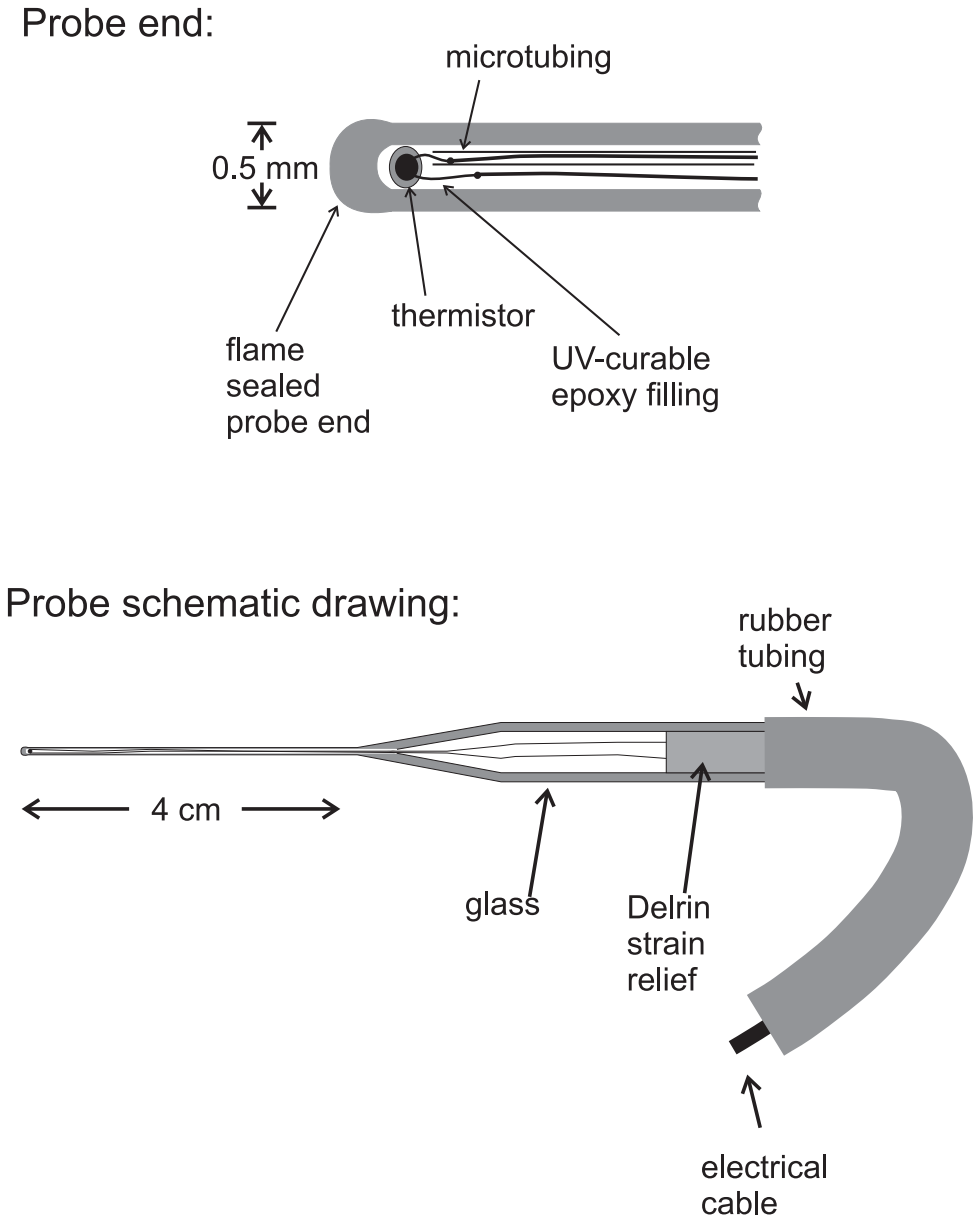

Figure 7: Drawing showing the details of the thermistor probes.

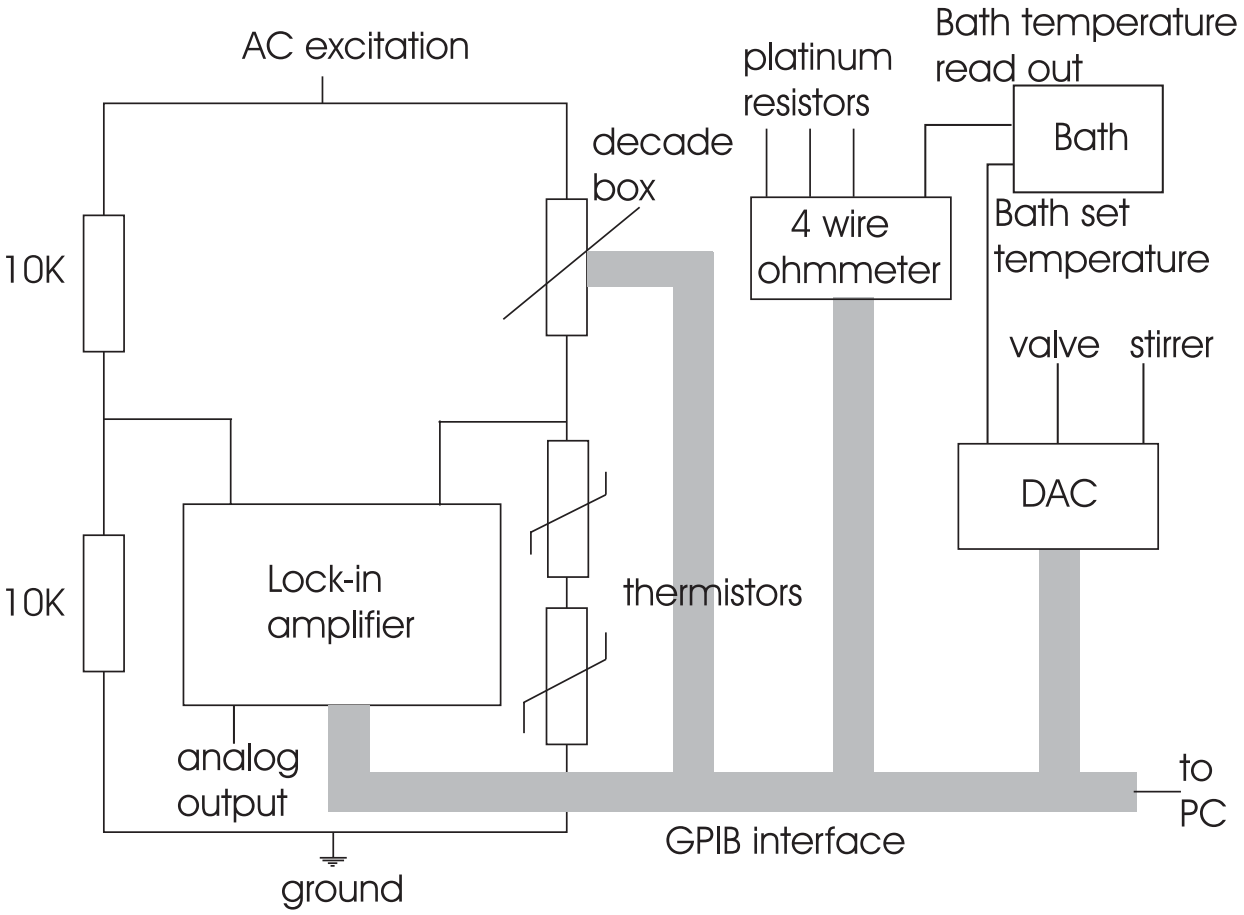

Figure 8: Schematic drawing of the electronics used with the water calorimeter. The lock-in amplifier, the decade box and the 4-wire ohmmeter can all be controlled and read out remotely. The stirrer, valve system and bath are also remotely controlled.

inum resistor probes, which are used for temperature monitoring, are connected to a remotely controlled scanning system (based on a Keithley 2001 multimeter equipped with a scanner card). The bridge balancing resistor, the lock-in amplifier and the multimeter are all connected to a PC using a GPIB interface card, thus allowing each to be controlled and read out remotely. The software allows the bridge to be balanced, the characteristics of the lock-in amplifier to be changed, the acquisition of data according to a preselected scheme and the calculation of the extrapolation curves and the dose. In addition, the stirrer, valve system and bath can be remotely controlled.

The drawing in figure 8 accurately reflects the configuration of the bridge at 22°C, when each thermistor has a resistance of approximately 5 kΩ. At 4°C, the thermistor resistance increases to approximately 10 kΩ, so the 10 kΩ decade box does not have enough range to permit the bridge to be balanced. To compensate, an extra 10 kΩ resistor is added in series with the decade box.

The response of the bridge per unit change in thermistor resistance is obtained by changing the resistance of the decade box by a known amount. A detailed electrical model of the bridge, including the impedances imposed by the lock-in amplifier, is used to relate the measured response to a change in the decade box to the response expected due to a change in the thermistor resistance. The 10 MΩ input impedance of the lock-in represents a significant loading of the bridge circuit, and its effect is largest when the bridge is asymmetric (4°C operation). If ignored, it can lead to errors of up to 0.3% in the estimated voltage change per unit change of thermistor resistance.

3 Determination of Absorbed Dose

The raw data obtained from a calorimeter run consists of the measured bridge voltage as a function of time. Changes in bridge voltage can be converted to changes in thermistor resistance, and these in turn can be converted to changes in temperature, if the thermistor sensitivity is known.

The approximate relationship between the thermistor resistance, R, and the absolute

temperature, T, is

$$R = R_0 e^{\beta(1/T - 1/T_0)}, \tag{2}$$

where R_0 is the thermistor resistance at temperature T_0, and β is a constant. In fact, β is not strictly constant, but is found empirically to change by about seven parts per thousand per degree. From equation 2 the thermistor sensitivity, S, defined by

$$S = \frac{\Delta R}{R}\frac{1}{\Delta T}, \tag{3}$$

can be shown to be given by

$$S = -\frac{\beta}{T^2}. \tag{4}$$

Once the temperature change, ΔT_{w}, is known, the absorbed dose to water, D_{w}, can be obtained from

$$D_{\mathrm{w}} = \Delta T_{\mathrm{w}} \cdot c_{\mathrm{w}} \cdot k_{\mathrm{c}} \cdot k_{\mathrm{v}} \cdot k_{\mathrm{p}} \cdot k_{\mathrm{dd}} \cdot k_{\rho} \cdot \frac{1}{1 - k_{\mathrm{HD}}}, \tag{5}$$

where c_{w} is the specific heat capacity of water, k_{c} and k_{v} are corrections for conductive and convective heat transfer, respectively, k_{p} is a correction for perturbations of the radiation field by the glass vessel or probes, k_{dd} is a correction for the non-uniformity of the lateral dose profile, k_{ρ} accounts for the change of the density of water with temperature and k_{HD} is the heat defect. The following sections describe briefly the thermistor calibration procedure and summarize our knowledge of the various correction factors.

3.1 Thermistor Calibration

Before use, the thermistor probes must be calibrated. The main requirement is that the probes accurately measure temperature *changes*, because detailed knowledge of the absolute temperature is not required for calorimetry. Our probes are calibrated against platinum resistance probes (RTDs) which in turn are calibrated against NRC temperature standards.

Accurate knowledge of a measured temperature change requires accurate knowledge of the thermistor constant, β. Domen (1994) has reported significant changes in β with time, thus emphasizing the importance of routine checking of the calibration factors. We have developed an automated calibration system in which the thermistors and RTDs are mounted in a separate Dewar containing a solution of 90% water and 10% ethanol. The temperature

of the solution in this Dewar is controlled using a bath running under computer control. The thermistor probes are protected against breakage by supporting each probe in a glass tube which is open at one end. The thermistor probes are connected to a Keithley K2001 multimeter through a scanner card, and measurements of the thermistor resistance are carried out using the instrument's 4-wire ohm mode (on the 200 kΩ scale, the bead power dissipation is about 0.5 μW). The Dewar water temperature and corresponding thermistor resistance is measured at a series of temperatures from -4 to 12°C (for calorimeter operation at 4°C) and from 14 to 30°C (for operation at 22°C). From these measurements, the thermistor sensitivity can be calculated. A full calibration for both temperature ranges for a set of three thermistors typically takes about 8 hours but virtually no human interaction is required once the system is running.

If equation 2 were an exact representation of thermistor response to temperature, then $\ln R$ would be linear with $1/T$. In fact, measured data are better represented by a second order polynomial of the form

$$\ln R = a_0 + \frac{a_1}{T} + \frac{a_2}{T^2}. \tag{6}$$

We note from equation 2 that

$$\beta = \mathrm{d}\ln R/\mathrm{d}(1/T),$$

and if applied to equation 6 gives

$$\beta(T) = a_1 + \frac{2a_2}{T}. \tag{7}$$

If equation 6 is recast in the form of equation 2 with β defined according to equation 7, then R_0 is no longer a constant, but is a weak function of T, given by

$$R_0(T) = \exp\left(a_0 + \frac{\beta(T)}{T_0} - \frac{a_2}{T^2}\right). \tag{8}$$

Of course, equation 6 could be used directly to calculate the thermistor sensitivity (equation 3) without introducing β and R_0. However, the temperature dependence of β and R_0 as given by equations 7 and 8 is quite weak and thus equation 2 (with β and R_0 constant) remains a useful starting point for estimating thermistor resistance and sensitivity.

Table 1 shows calibration data for six thermistor probes. The calibrations were separated by six to nine months and any variations in β were less than 0.1%. This suggests that our

Probe No., Op. Temp.	Time of calibration			
	May 1996	Jan.-Feb. 1997	Mar. 1997	Sep. 1997
1, 4°C	3111.20(4493.62)	3113.97(4480.99)		
1, 22°C		3156.41(4453.01)		
2, 4°C		3054.52(4312.02)		
2, 22°C		3090.96(4287.25)		
3, 4°C	3075.43(4258.48)	3074.94(4236.82)		
3, 22°C		3121.37(4225.30)		
4, 4°C			3109.53(4378.32)	3108.96(4381.13)
4, 22°C			3150.05(4351.40)	3152.90(4352.32)
5, 4°C			3060.46(4526.75)	3059.65(4527.68)
5, 22°C			3099.05(4500.39)	3100.64(4499.98)
6, 4°C			3111.09(4421.75)	3110.47(4422.93)
6, 22°C			3152.77(4394.52)	3154.66(4394.06)

Table 1: Thermistor material constants measured at different times. Probes 1 to 3 were constructed in the spring of 1996, and had failed by January, 1997. Probes 4 to 6 were constructed in the spring of 1997. Thermistor 5 has not yet been irradiated. The values of β and R_0 (in parentheses) were obtained using equations 7 and 8. The reference temperature, T_0, was taken to be 25°C (298.15 K), and β is expressed in degrees (Kelvin) and R_0 is in ohms.

probes do not show the same variations in sensitivity as observed by Domen (1994), but more calibration sets are required before we can be confident of their stability.

Because of the electrical energy dissipated in the bead, the temperature of the bead is higher than that of the water. This temperature difference is an indication of the quality of the thermal coupling between the bead and the water. The excess bead temperature is obtained by measuring the change in thermistor resistance as the thermistor power is changed. We find that the bead temperature rises by about 1.9 mK per μW of power

dissipated in the bead.

If the thermistor power is high, Domen (1982) showed that the change in thermistor resistance during an irradiation run can be large enough to change significantly the thermistor power and, thus, the temperature difference between the bead and the water. If not corrected for, this change in temperature would erroneously be interpreted as part of the temperature change caused by the absorbed dose. Our measured data are corrected for this effect, although it is negligible (less than 0.1%) for our standard operating power level of 6.2 μW.

3.2 Transient Thermistor Response to Radiation

Domen (1994) has reported on results obtained at NIST which show that thermistors can tolerate doses of several MGy with no adverse effects. Calorimetric measurements of the absorbed dose for radiation therapy purposes are unlikely to require doses of more than a few kGy. Thus, we can safely assume that radiation will have no effect on the quiescent behaviour of our thermistor probes.

However, there remains the possibility that radiation might induce transient effects which persist for tens of seconds and thus distort the post-irradiation drift curve. To test this possibility, we constructed the apparatus shown in figure 9. Two closely matched thermistors were placed in a flow of temperature-regulated water. The thermistors were mounted in opposite arms of a Wheatstone bridge so that the output voltage was close to zero when water was flowing over the probes. A collimated electron beam was used to irradiate one of the thermistors while the second remained in a field-free region. Because of the flowing water, both probes continued to see approximately the same temperature, and any transient effects after the beam was turned off would be due to radiation-induced changes in the thermistor response. Measurements were carried out at 4°C and 22°C.

The results are summarized in figure 10. The dose rate from the electron beam was approximately 150 Gy/min, which would give a temperature rise of about 60 mK in 100 s in stagnant water. This would correspond to a signal of approximately 460 μV in figure 10. The radiation-induced signal when the beam was on amounted to 1 or 2 μV and was due to local heating of the water and probe. However, any transient effects were over in less than

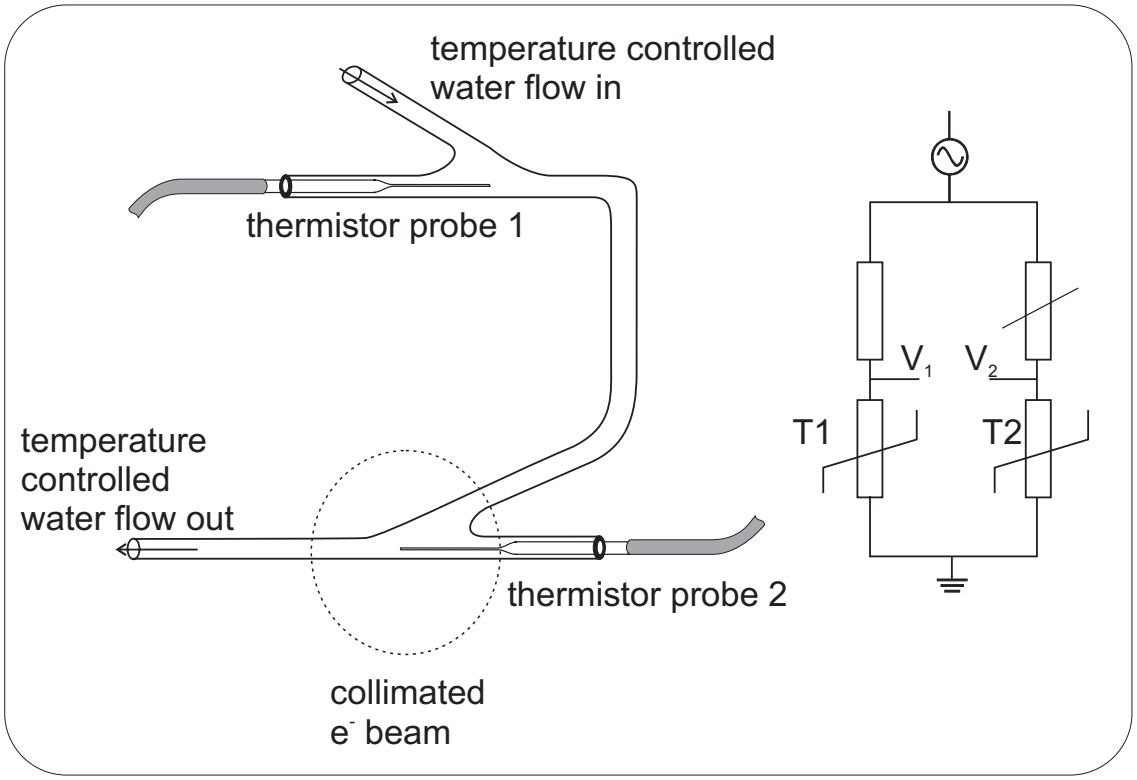

Figure 9: Schematic of the setup used to measure the transient response of thermistors to radiation. The same temperature-regulated water flowed over both thermistor probes. The whole assembly was insulated from the environment using Styrofoam sheets. One thermistor was irradiated with a high dose rate (150 Gy/min) electron beam and the difference in response of the two thermistors was measured. The bridge circuit on the right shows how the difference signal was obtained by placing the thermistors in opposite arms of a Wheatstone bridge.

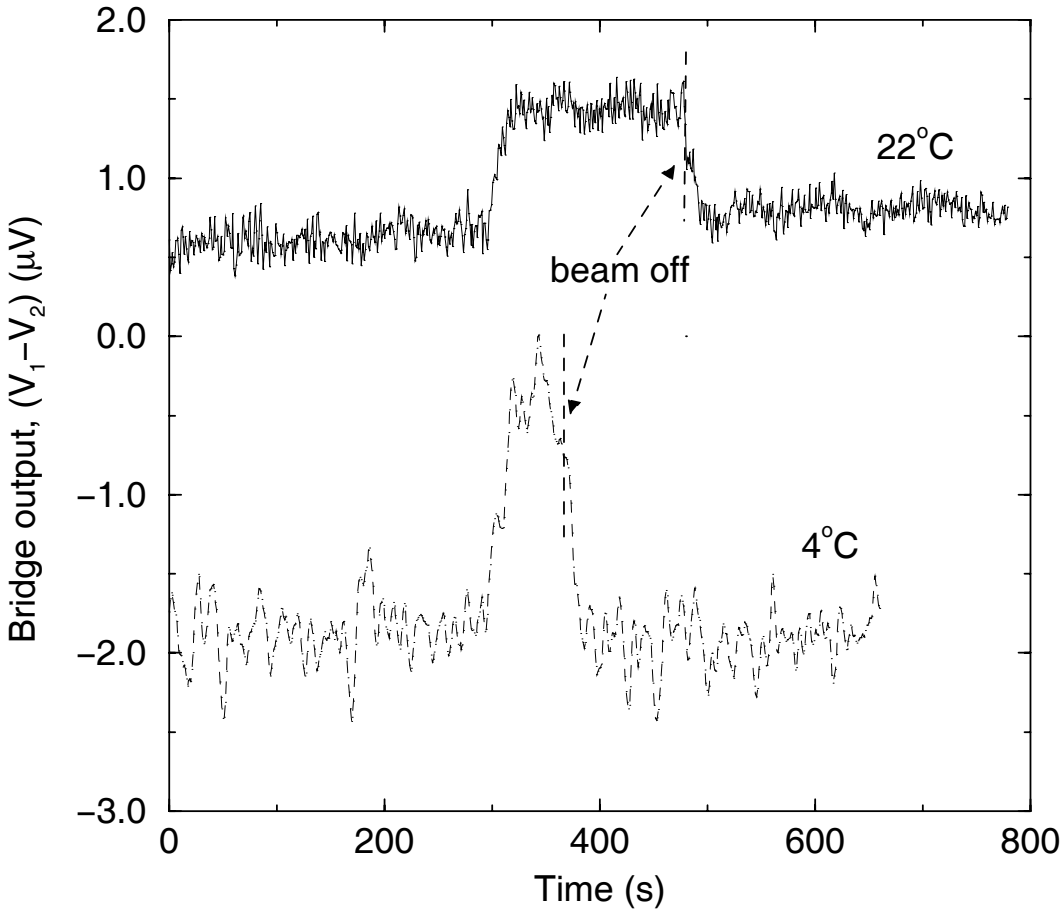

Figure 10: Measured transient response of a thermistor to radiation. The electron beam dose rate was approximately 150 Gy/min, and measurements were carried out at both 4°C and 22°C. A 1 μV change in bridge output corresponds to a temperature change of approximately 130 μK, and in 100 s the signal would have been about 460 μV if the water had been stagnant.

20 s after the beam was turned off, and were less than 0.5 μV, or 0.1% of the signal due to the absorbed dose in stagnant water. Assuming that thermistor response is not altered by dose or dose rate, these results show that any transient change in thermistor response should not affect the measured absorbed dose under normal operating conditions by more that 0.1%.

3.3 Conductive Heat Transfer

Conductive heat losses in a large water calorimeter may result from two sources. Firstly, because the heat capacity of glass is about one-sixth that of water, the radiation-induced temperature rise in the glass would be about six times that in water, if it were not that most of the heat generated in the glass is transferred to the water. Secondly, temperature gradients within the water because of non-uniformities in the absorbed dose distribution will lead to conductive heat transfer. We now examine each of these effects in more detail.

To calculate the effect of heat transfer from the glass we use the following simplifying assumptions: the calorimeter is irradiated uniformly; the glass vessel is an infinitely long cylinder; the thermistor bead is located symmetrically at the end of the glass probe; each probe is semi-infinite in length. Under these assumptions, rotational symmetry reduces the problem to two dimensions. This two-dimensional space is divided by an irregular rectangular grid with a high resolution in the neighbourhood of the probe, probe tip and vessel, and a low resolution elsewhere. Heat transfer calculations begin at the start of the irradiation. For every rectangular cell of the grid the transport of heat energy is calculated in discrete time steps. The calculated effect on the temperature at the point of measurement can either be subtracted from the measured signal before the run is analysed, or the run can first be analysed to get an approximate temperature change which is then corrected for the effects of heat conduction. Additional details have been reported by Seuntjens and Palmans (1999).

The calculated excess temperature rise in a ^{60}Co beam, for the NRC geometry and for different irradiation times, is plotted in figure 11 for vessel dimensions similar to those of vessel #1. Results for vessels similar to vessel #3 are shown in figure 12. The decrease in temperature immediately after the irradiation is caused by excess heat from the probe that is conducted away from the probe axis into the water, while the increase in temperature at later

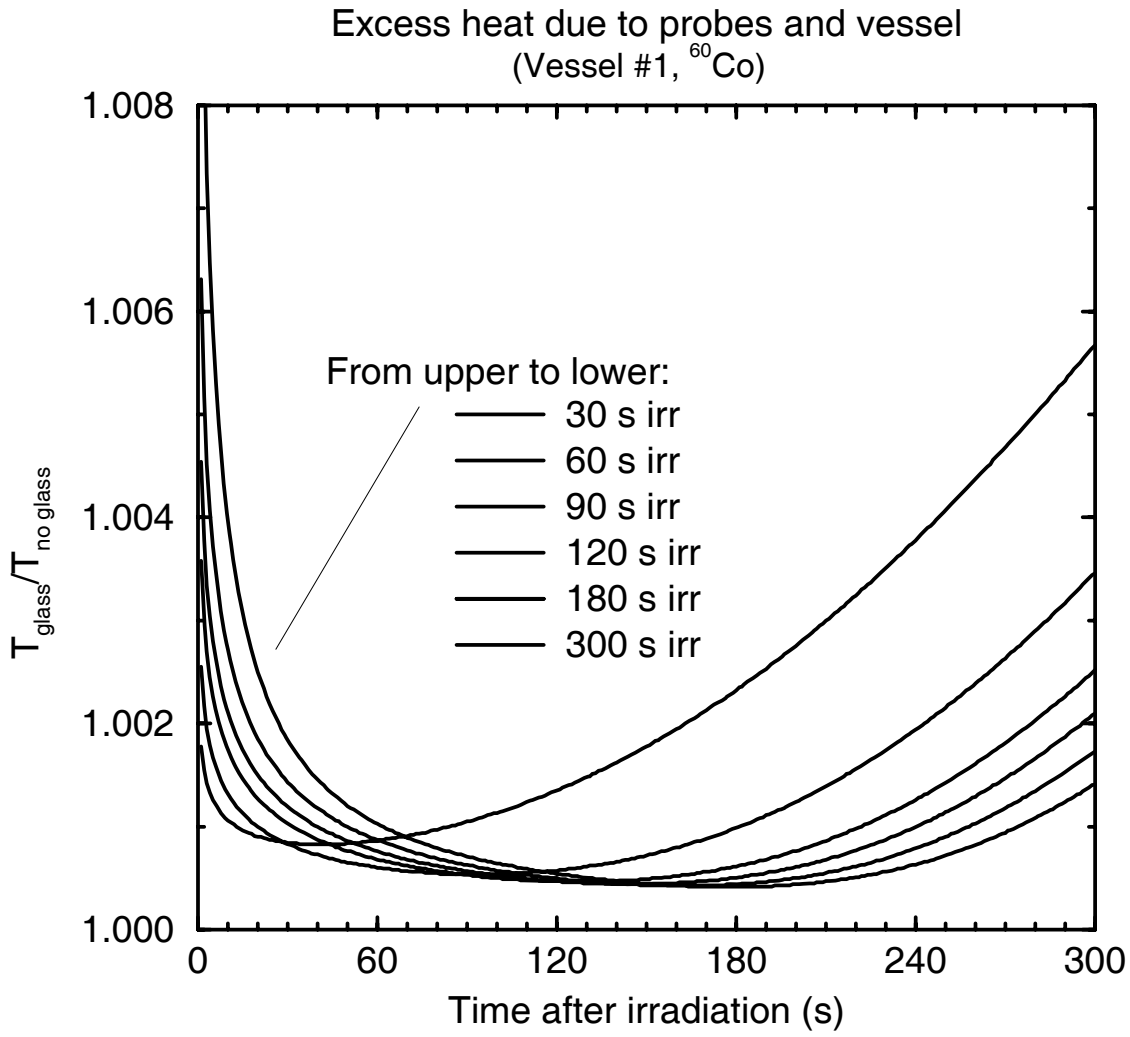

Figure 11: Calculated excess temperature at the end of each thermistor probe, caused by heat conduction from the probes and from the vessel wall. The results apply for vessels with dimensions similar to those of vessel #1. The decrease in temperature immediately after irradiation is due to heat flowing away from the probes. The increase in excess temperature several minutes after the irradiation is due to heat produced in the vessel wall and transported to the point of measurement.

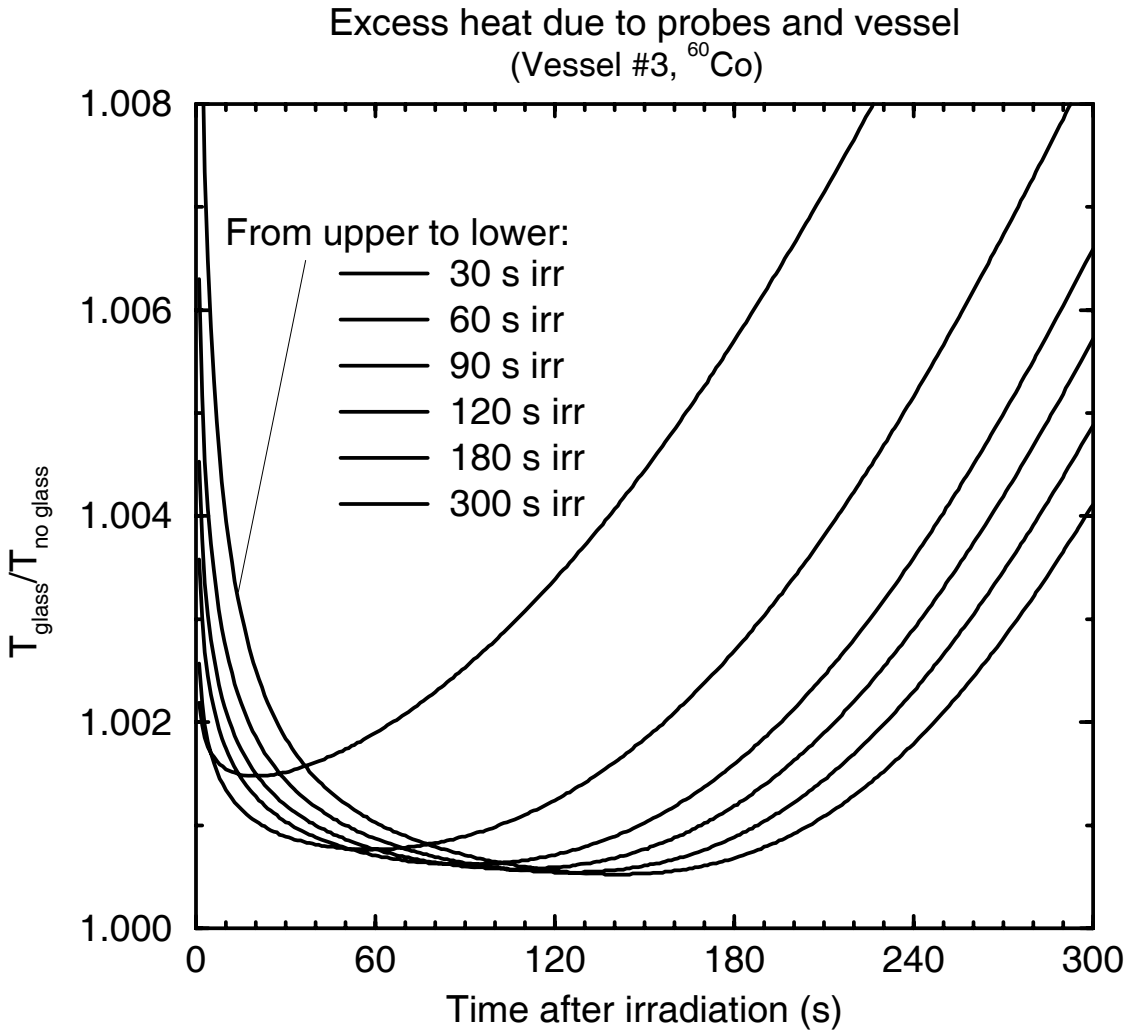

Figure 12: Same as figure 11, but for vessel #3.

times is due to excess heat from the vessel reaching the probes. Table 2 gives a summary of

Irradiation time (s)	Post-irradiation drift interval (s)				
	30	60	120	180	240
30	-0.36	-0.29	-0.21	-0.17	-0.14
30	-0.36	-0.29	-0.21	-0.16	-0.08
60	-0.30	-0.24	-0.18	-0.14	-0.10
60	-0.30	-0.24	-0.17	-0.11	-0.07
90	-0.27	-0.21	-0.16	-0.12	-0.07
90	-0.27	-0.21	-0.14	-0.07	+0.04
120	-0.24	-0.20	-0.14	-0.09	-0.04
120	-0.24	-0.19	-0.14	-0.01	+0.11
180	-0.21	-0.16	-0.10	-0.03	+0.04
180	-0.18	-0.12	-0.01	+0.12	+0.27

Table 2: Calculated correction factor, k_c, expressed as %, on the linear extrapolation to mid-run due to excess heat produced in the end of thermistor probes and in the vessel wall for vessels with dimensions similar to those of vessels #1 and #3. A positive value for the correction means the temperature rise obtained by linear extrapolation should be increased accordingly. Calculations were performed for different irradiation times and for different intervals used to specify the post-irradiation drift curve. The first and second row for each irradiation time is for vessels #1 and #3, respectively. The post-irradiation drift interval starts 20 s after the end of the irradiation.

calculated values of k_c for vessels #1 and #3. For 180 s irradiations with probes of 0.5 mm diameter, corrections of less than 0.2% are calculated for fits of the post-irradiation drift in the range of 30 to 180 s.

For beams of ^{60}Co γ-rays or high energy x-rays, the largest dose gradients occur in the buildup region or at the edges of the field. If calorimeter measurements are restricted to depths beyond the dose maximum, and if the field size is reasonably large (10 cm by

10 cm or larger), then the effect of conductive heat transfer due to dose nonuniformities is very small (Roos 1988; Seuntjens 1991). However, dose gradients are much more severe for electron beams and conductive heat transfer can be a problem. Although our current efforts are directed towards the use of the sealed water calorimeter for high-energy photon beams, some initial calculations of the effect of conductive heat transfer in a 15 MeV electron beam are presented in figure 13. These preliminary results suggest that water calorimetry should also be feasible for high-energy electron beams.

3.4 Convective Heat Transfer

In addition to heat transfer by conduction, heat transfer by convection can occur in a liquid calorimeter. If the water in the calorimeter is heated nonuniformly, buoyant forces will arise due to local density changes in the gravitational field. These forces may lead to flow within the liquid, and this flow will contribute to heat transport. The flow rate may depend on the absorbed dose and on time, and thus the effective heat transfer coefficient at the point of measurement will not be constant. Under these conditions, the standard approach of extrapolating initial and final drifts to mid-run (Laughlin and Genna 1966) may not accurately account for convective heat transfer.

Convection in a water calorimeter can be caused in different ways. It can arise at locations of sharp temperature gradients caused by uncontrolled temperature changes in the environment, or by gradients due to successive irradiations (Domen 1987). Depending on construction details of the probes, sharp temperature gradients may be present in the vicinity of the thermistor probe ends due to the dissipation of electrical power in the thermistors. It can also be caused when non-water materials in direct contact with the water produce excess heat when irradiated (e.g., the Lucite window).

Schulz and Weinhous (1985) pointed out that one way of avoiding altogether the onset of convection is to operate the calorimeter at 4°C, because at this temperature the volume expansion coefficient of water is zero. Schulz *et al* (1987), (1991) constructed a calorimeter which could operate at 4°C and used it to perform detailed absorbed dose measurements. Our calorimeter can be operated at any temperature from 0°C to about 30°C and by operating at both 4°C and room temperature, one can check for systematic effects due to convection.

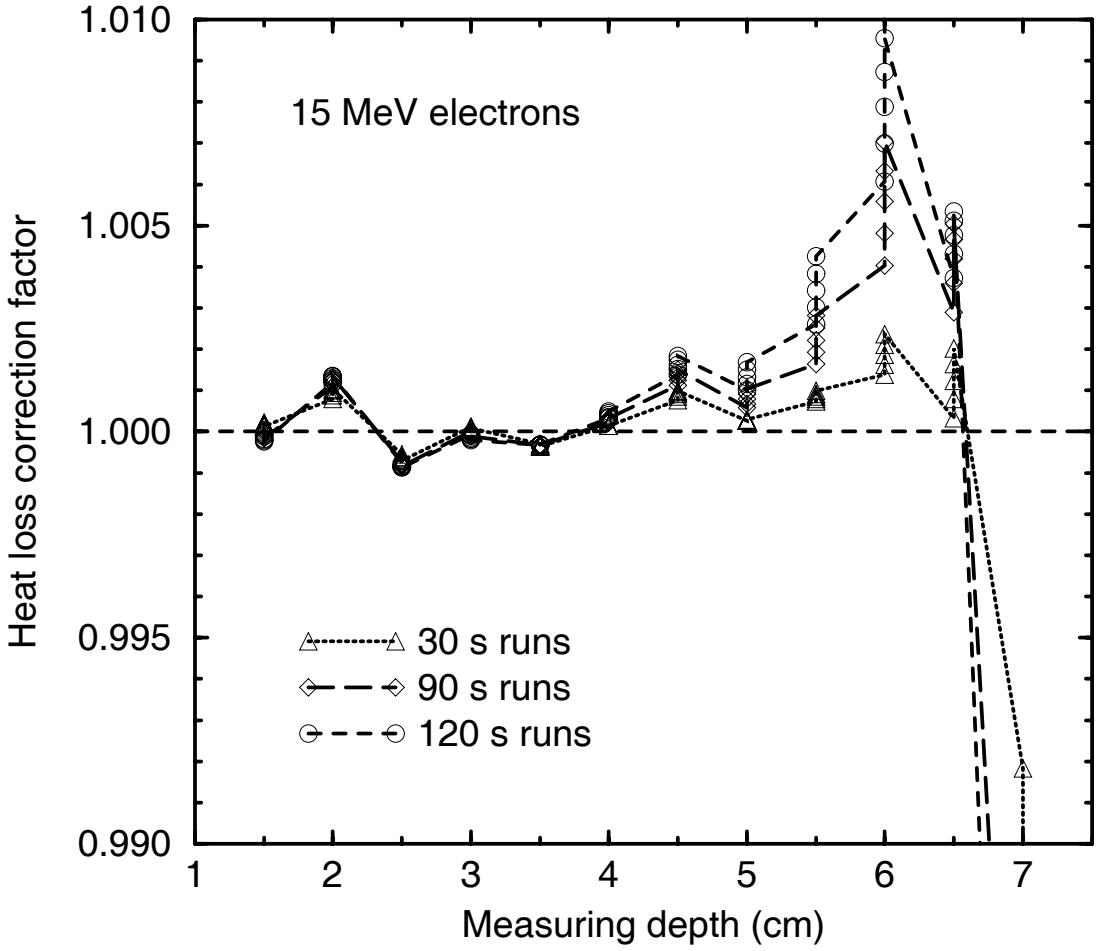

Figure 13: Calculated conductive heat-loss correction due to dose gradients in a 15 MeV electron beam as a function of the depth of the measuring point. The peak of the depth dose curve is at about 2.5 cm. The correction was calculated for several irradiation times, as indicated by the different symbols. The series of identical symbols at each depth shows the effect of using different time intervals (30 to 120 s) to characterize the post-irradiation drift.

It may also be desirable to investigate further the onset of convection around the tips of the probes. Domen (1988) studied this problem using forced convection, and concluded that there was no evidence for thermistor-induced convection for power levels below 50 μW. On the other hand, Seuntjens (1991) presented data that suggested that convection may be present for thermistor powers as small as 5 μW.

We assume that k_{v} in equation 5 is unity when the calorimeter is operated at 4°C. Data presented later in this report indicate that k_{v} may be about 0.993 at 22°C for our vessel configuration.

3.5 Radiation Field Perturbation

The presence of the calorimeter detection vessel and the glass thermistor probes perturbs to some extent the radiation field when compared to the situation where these objects are absent. The perturbation of the ^{60}Co radiation field by the vessel has been measured using a PTW-M233642 ionization chamber, and amounts to 1.0021 $\pm$ 0.0005. Since 0.9 mm of glass would attenuate the ^{60}Co beam by about 0.6%, these measurements show that photon attenuation in the glass is partially compensated by the slightly increased dose contribution from scattered photons when the vessel is present. This observation was confirmed by performing a correlated sampling Monte Carlo simulation of the photon transport through the water phantom. By scoring the fluence in a spherical region on the beam axis at the position of the centre of the vessel with the vessel and probes absent and with both materials present, the correction factor was found to be 1.0028 $\pm$ 0.0008, in good agreement with the measurements. Using the same measuring technique we determined $\mathrm{k_p}$ to be 1.0015 $\pm$ 0.0002 at 20 MV.

3.6 Dose Profile Non-Uniformity

The lateral profile of the dose in the x-y plane perpendicular to the beam axis at the measuring point is slightly non-uniform depending on the field size and the source detector distance. We measured the x-y dose profile using a PTW-M233642 ionization chamber with a cavity volume of 0.125 cm^3, and used these data to calculate the correction factor, k_{dd}, required

to obtain the dose at a point on the beam axis. For the calorimeter, $k_{\rm dd}$ is 1.0004 for ^{60}Co γ-rays and 1.0012 for 20 MV x-rays and depends slightly on the separation of the probe ends. For the standard quartz Fricke vials the corresponding results are 1.0021 for ^{60}Co γ-rays and 1.0035 for 20 MV x-rays.

3.7 Density of Water

For practical reasons, ion chamber measurements need to be done at room temperature. If the calorimetry measurements are done at 4°C, a small correction, k_ρ, is necessary to determine the dose at 22°C. Because the density of water increases by 0.22% as the temperature decreases from 22°C to 4°C, there will be more water overlying the measuring point at 4°C than at 22°C. Taking the dose gradient for ^{60}Co to be 5%/cm, the extra attenuation at the calibration depth of 5 cm will be approximately 0.055%, leading to a value for k_ρ of 1.00055.

In order to estimate k_ρ for 20 MV x-rays, we have taken the depth-dose distribution measured at 22°C and scaled the depth axis so that $x' = x/1.0022$. This leads to a value for k_ρ of 1.0010 at the calibration depth of 10 cm.

3.8 Heat Defect

The use of calorimetry to measure absorbed dose is complicated by the fact that the measured heat energy may not correspond to the energy absorbed from the radiation field. The heat defect is used to quantify the difference between the energy absorbed, $E_{\rm a}$, and the energy appearing as heat, $E_{\rm h}$, and it is defined by

$$k_{\rm HD} = \frac{E_{\rm a} - E_{\rm h}}{E_{\rm a}}. \tag{9}$$

The heat defect is positive for endothermic processes, while it is negative if the radiation induces exothermic processes in the calorimeter. For water irradiated by low LET radiation, the heat defect is almost entirely due to radiation-induced chemical reactions (Ross *et al* 1989).

The heat defect can be calculated using the established model for the radiolysis of water. In this model, the ionizing radiation first produces localized clusters of reactive species, called

spurs. After about 0.1 μs, the spur products act as if they are homogeneously distributed, and are assigned yields, G_i, where the subscript, i, identifies the species. The concentrations of the spur products and other reactive species within the aqueous solution are followed using homogeneous reaction kinetics, where the reactions involved, the rate constants and the values of G_i are obtained from the published literature on the radiolysis of water. In general, there will be n species which participate in m reactions. The rate constant for reaction i is denoted by k_i, and for the aqueous systems we have studied to date, only first and second order reactions are involved. Mathematically, the problem is equivalent to solving a set of coupled first order differential equations of the form

$$\frac{\mathrm{d}C_i}{\mathrm{d}t} = \rho G_i \dot{D} - \sum_{1^{st},C_i\downarrow} k_j C_i - \sum_{2^{nd},C_i\downarrow} k_j C_i C_k + \sum_{1^{st},C_i\uparrow} k_j C_k + \sum_{2^{nd},C_i\uparrow} k_j C_k C_l. \qquad (10)$$

The concentration of species i is given by C_i, and there are n equations similar to equation 10. The first term in the equation gives the production rate of species i due to spur reactions, where ρ is the density of water and $\dot{D}$ is the dose rate. The labelling "1^{st}" and "2^{nd}" on the sums indicate that they are to be taken over all relevant first and second order reactions, respectively, while "$C_i\downarrow$" and "$C_i\uparrow$" indicate that they are to be taken over all reactions in which species i is being consumed or produced, respectively. Specific values for the initial yields and rate constants can be found in Klassen and Ross (1991).

At a specified time after the irradiation, the yield of species i can be expressed as G'_i, where the prime is used to distinguish it from the yield at 0.1 μs. Then the heat defect is calculated using

$$k_{\mathrm{HD}} = \sum_{i=1}^{n} G'_i \cdot \Delta H_i, \qquad (11)$$

where ΔH_i is the heat of formation for species i. Note that G'_i can be negative or positive.

The model calculations can be tested experimentally by comparing the relative response of different aqueous systems. Klassen and Ross (1991) have identified several aqueous systems which are suitable for water calorimetry. These include pure water, water saturated with H_2 gas and water saturated with a 50/50 mixture of H_2 and O_2 gases.

In general, both G_i and k_i depend on temperature. Because the calorimeter is operated at both 4°C and 22°C, the temperature dependence of the heat defect must be estimated. For those systems which attain a steady state after some modest accumulated dose, the

situation is quite straightforward. The only concern is whether or not the accumulated dose required to reach steady state (and thus zero heat defect) depends on the temperature. Using data from Elliot (1994) on the change of G_i and k_i with temperature, the heat defect for H_2-saturated and pure water was calculated for a dose rate of 1.5 Gy/min at 4°C and 22°C. At both temperatures, the heat defect after an accumulated dose of 3 Gy was less than 0.1%. Furthermore, the reactions go to completion almost immediately after the irradiation stops.

The situation is more complicated for water saturated with H_2 and O_2 gases. This system is exothermic over a wide range of accumulated dose, and requires that the heat defect be calculated as a function of dose rate and accumulated dose. Although this might be seen as a significant disadvantage, it is largely outweighed by the fact that earlier work (Klassen and Ross 1991) had shown that H_2/O_2 water is insensitive to impurities. Furthermore, various tests (Klassen and Ross 1997) indicated that the standard model for the radiation chemistry of water was sufficiently well established so as to introduce no significant uncertainty into the calculated heat defect.

This perspective has been called into doubt by some recent work based on a revised model for the radiolysis which shows that the reactions take more than 100 s to go to completion (Klassen and Ross 1997). This means that the final drift interval will have some curvature, thus complicating the standard procedure of estimating heat losses by extrapolating to mid-run. Figure 14 shows how the calculated effective exothermicity depends on irradiation temperature and on the time after irradiation. Earlier models for the radiolysis showed that the exothermicity was within 0.2% of its final value within the first 20 s after irradiation. The reasons for this difference are presently not known but are under investigation.

4 Calorimeter Performance

Figure 15 shows the response of the NRC calorimeter to ^{60}Co γ-rays at a dose rate of about 1.5 Gy/min. The calorimeter was operated at 4°C, and the power dissipated in each thermistor bead was 6.2 μW. The irradiation time was 120 s, and 120 s of pre- and post-irradiation drift is shown. The resistance change of the thermistors corresponding to this measurement amounted to 0.56 Ω on a total resistance of 19,000 Ω. In the inset, the bridge

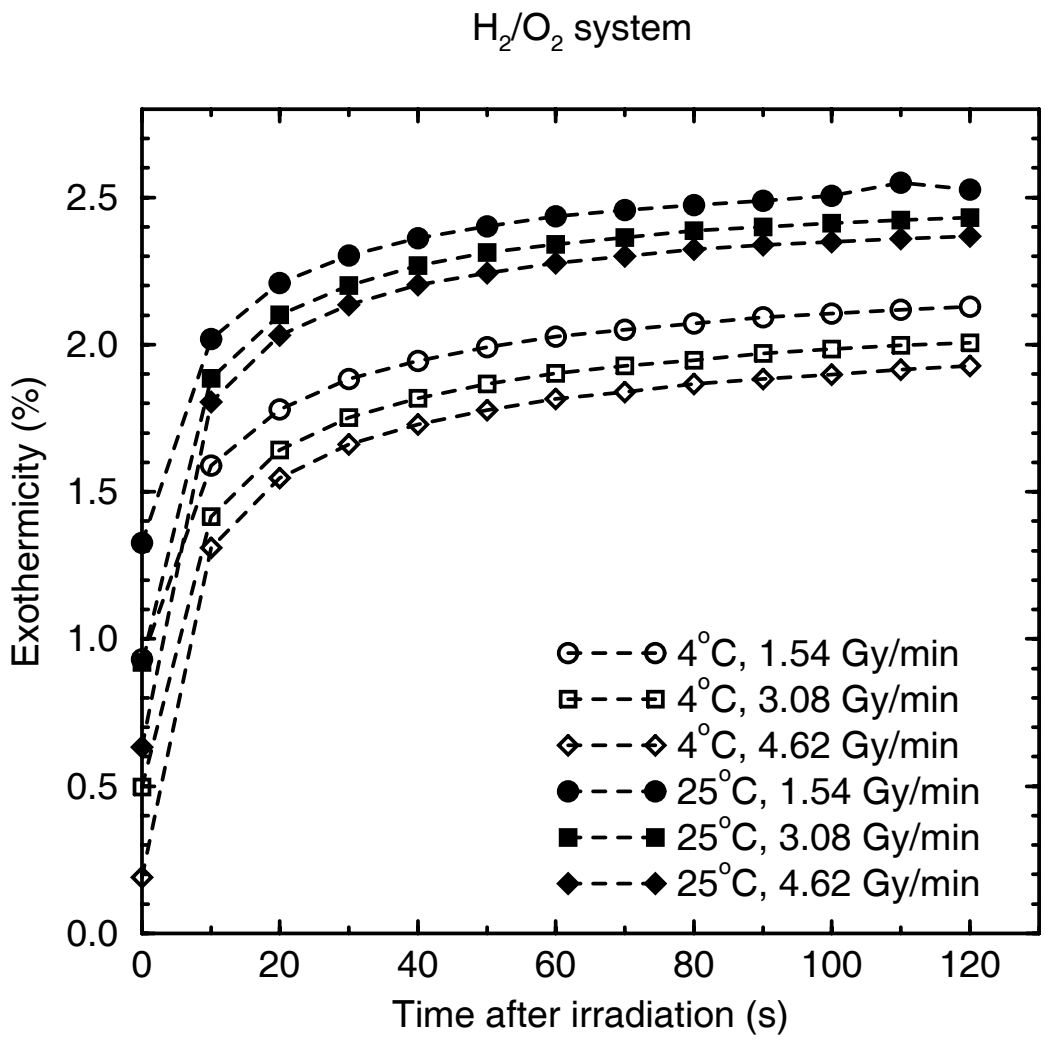

Figure 14: Effect of the irradiation temperature on the calculated heat defect (expressed as percent exothermicity) of water saturated with a 43/57 mixture of H_2 and O_2 gases. Results are shown for three different dose rates, but the irradiation time was adjusted so that the same dose was delivered in each case.

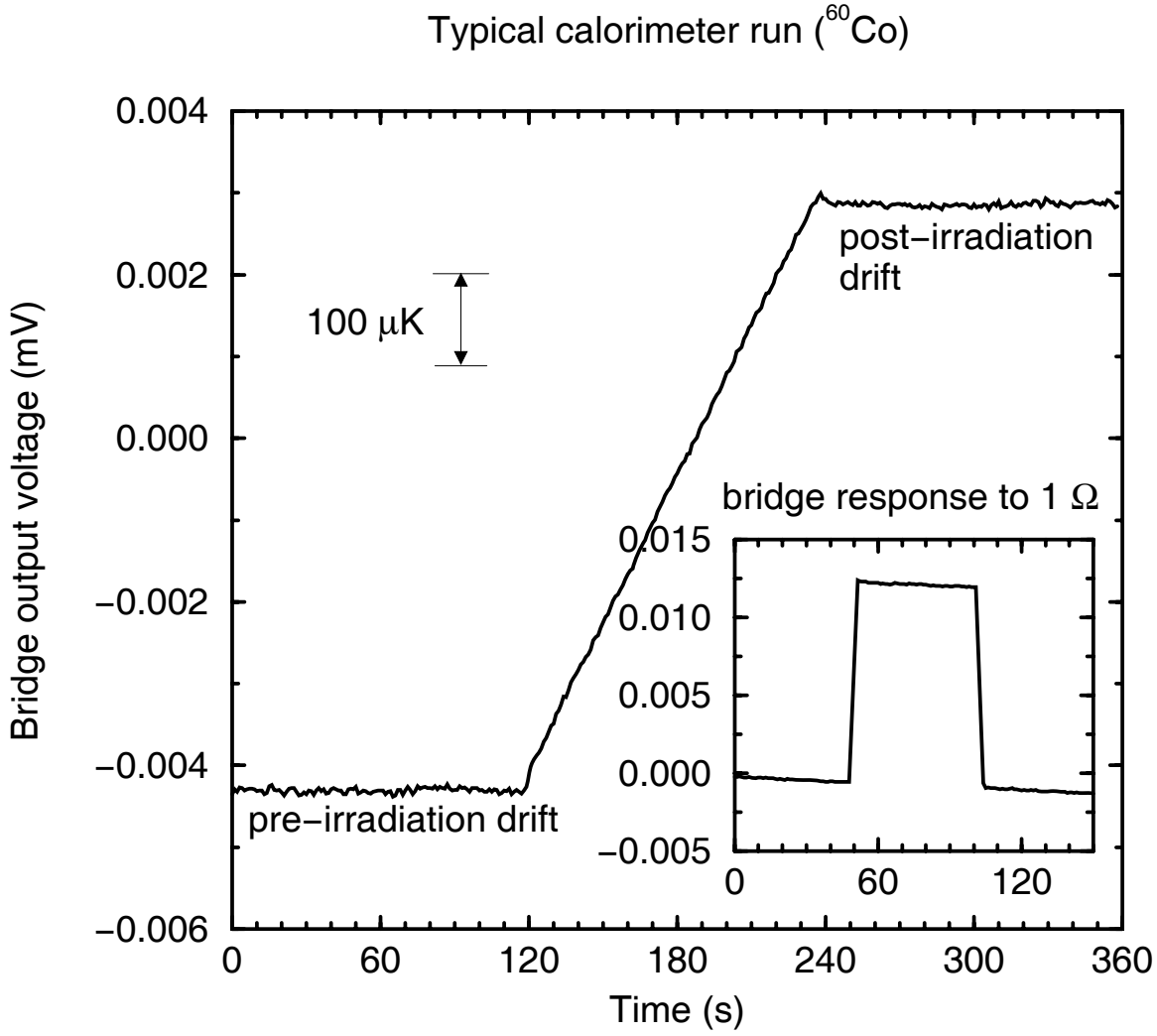

Figure 15: Sealed water calorimeter run (120 s) obtained using ^{60}Co γ-rays. In the inset, the response to a 1 Ω increase in the decade box resistance is shown. This corresponds to about twice the radiation induced signal.

response to an increase of 1 Ω in the bridge arm opposite to the thermistors is shown. By analysing the bridge circuit, this change can be related to a corresponding change in the total thermistor resistance. Tests for reproducibility of the calorimeter response showed that, for 120 s runs, the sample standard deviation (obtained from a set of 7 to 11 runs) was 0.7 to 0.8%. If the irradiation times were shorter, i.e., 90 s or 60 s, the sample standard deviation was 0.9% and 1.7%, respectively.

Figure 16 shows an expanded view of the noise level on a pre-irradiation drift curve just before a 90 s irradiation run. The amplitude of the noise signal converted to equivalent temperature amounts to about 10 μK (a typical run leads to a temperature change of about 700 μK) and the pre-irradiation drift rate (heating) is 0.51 μK/s.

Figure 15 shows a sudden, but small, change in response when the radiation beam is turned on and off. The effect can be made substantially larger by irradiating various components of the bridge circuit. More recent work has shown that this jump was due to a combination of ground loops and improper cable shielding in the bridge circuit. The present bridge configuration shows no such beam-related transient response, but there is no evidence that the transient had any impact on the measured absorbed dose.

5 Relative Absorbed Dose Measurements

The measurement of absorbed dose using water calorimetry requires a correction for the heat defect of the aqueous system used in the calorimeter. We tested the calorimeter response at ^{60}Co for several aqueous systems, including water saturated with Ar or N_2 gas (i.e., pure hypoxic water), water saturated with a mixture of H_2 and O_2 gases in a ratio 43/57, and water saturated with H_2 gas. The water used was purified using a Milli-Q UV Plus water purifier. The results were obtained using vessel #1 and are summarized in figure 17.

The H_2/O_2 gas mixture system, at the indicated ratio, is calculated to produce an exothermic heat defect which is approximately constant up to 400 Gy and amounts to 1.6%[1]. The other two systems are expected to produce a zero heat defect. Each of the points in the

[1]These calculations were based on the model referred to as Model III in Klassen and Ross (1997), and include an estimate of the effect of the sluggish approach to equilibrium (figure 14).

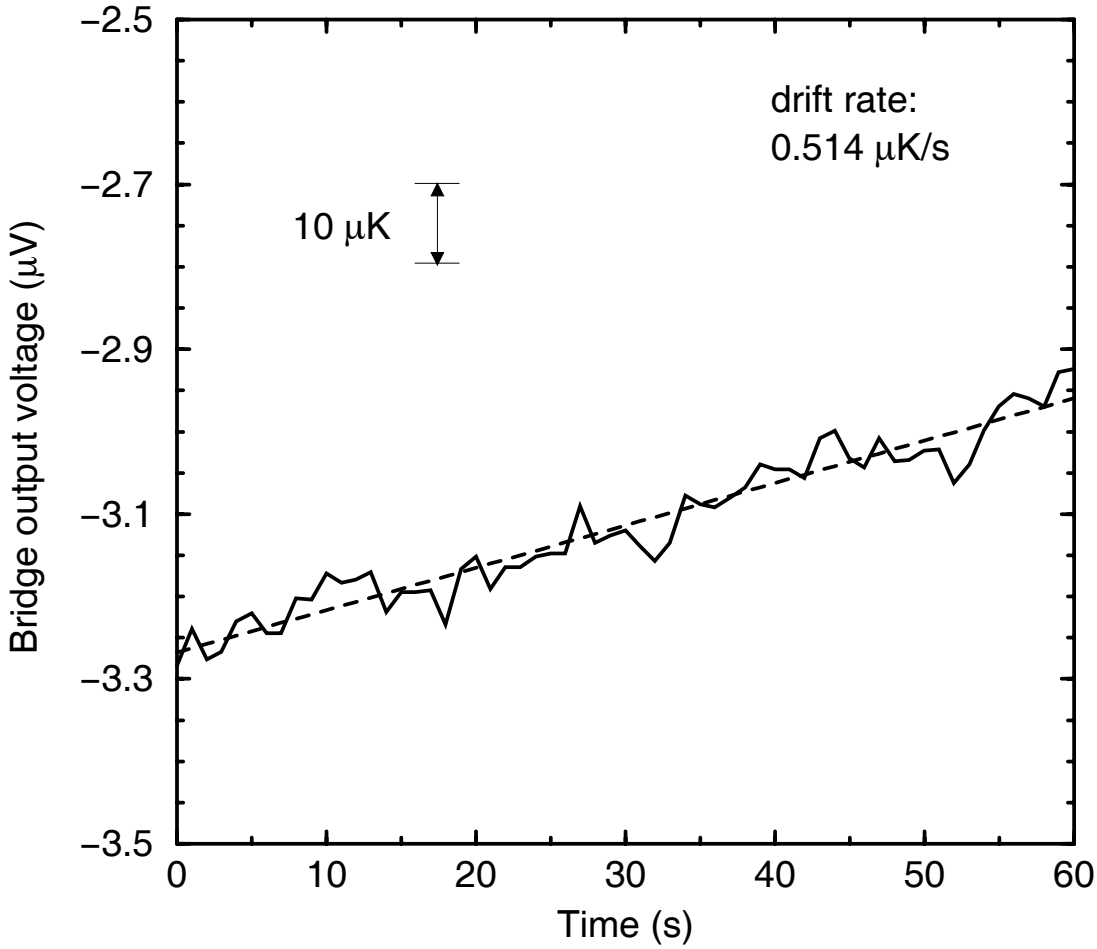

Figure 16: Typical calorimeter noise and drift performance.

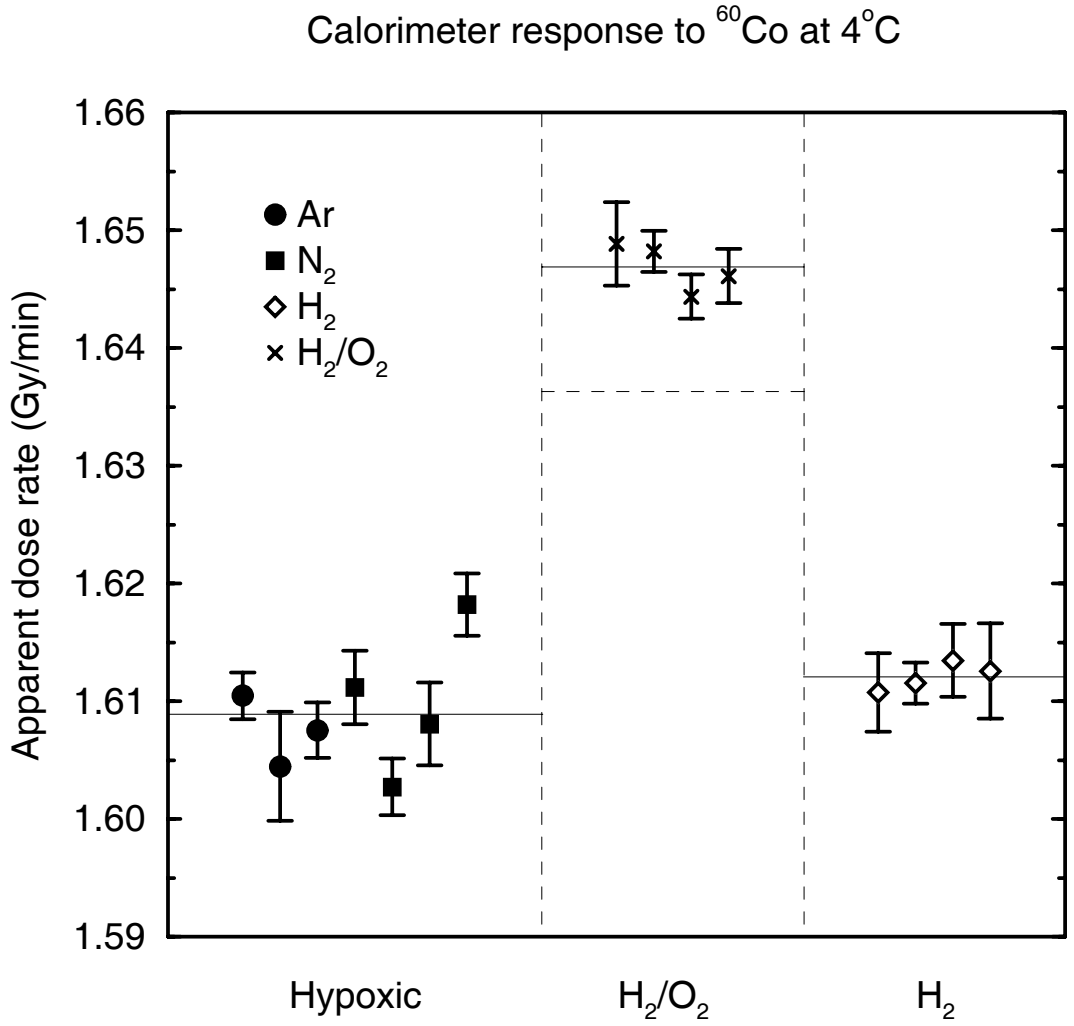

Figure 17: Summary of results obtained using the sealed water calorimeter and three different aqueous systems. The measurements were done using ^{60}Co γ-rays, with the calorimeter operating at 4°C. The ordinate is labelled "Apparent dose rate" because no heat defect correction was applied to any of the measured results. The solid horizontal lines represent the mean values of each data set. The dashed horizontal line is the predicted result for the H_2/O_2 system.

figure represents the average of a number of measurements (7 - 20 individual runs). Each run was corrected using the heat-loss correction discussed in section 3 and the averages are corrected for decay to refer to the dose rate of the NRC ^{60}Co source on October 1, 1996.

The pure hypoxic water measurements were performed twice, once using Ar-saturated water and once using N_2-saturated water. With these systems, after an initial settling period, there was no significant dose dependence of the calorimeter response although the individual measurement sets, performed at different accumulated doses, differed by up to 0.5%. The H_2 system also showed an initial dose dependence which is usually associated with removal of traces of oxygen. The measurements with the H_2/O_2 mixture were performed at low dose as well as after about 100 Gy accumulated dose, and showed no significant dose dependence.

The full lines in figure 17 represent the averages of each of the systems for which the numerical values are summarized in table 3. The horizontal dashed line is the model prediction

Chemical system	Apparent dose rate in Gy/min (Oct. 1, 1996)	% diff. from pure water	Heat defect (%) (model calc.)
pure water	1.609 ± 0.16%	0.0	0.0
H_2/O_2	1.647 ± 0.06%	2.3	1.6 (exo)
H_2	1.612 ± 0.10%	0.2	0.0

Table 3: Summary of results obtained using three aqueous systems, i.e., pure hypoxic water (Ar or N_2 saturated), H_2/O_2 (43/57) mixture and H_2 saturated water at 4°C. The heading of column 2 is labelled "Apparent dose rate" because the measurements have not been corrected for the heat defect. The indicated uncertainties (one standard deviation) exclude systematic uncertainties associated with the heat defect, heat loss correction factors, positioning, and thermistor calibration.

for the H_2/O_2 system (assuming zero heat defect for the other systems) and lies about 0.7% below the measured response. Earlier models for the radiolysis of water (Klassen and Ross 1991) give results which are in much better agreement with experiment. The differences between the various models which lead to this discrepancy are under investigation but for

the present work we use the heat defect predicted by the most recent model.

6 Comparisons of Absorbed Dose for ^{60}Co

The first NRC standard for absorbed dose to water due to ^{60}Co γ-rays was based on graphite calorimetry (Henry 1977). The dose has also been measured using Fricke dosimetry which was calibrated using stirred water calorimetry. In this section, the value of the absorbed dose obtained using the new, sealed water calorimeter will be compared to the values of dose obtained previously.

6.1 Dose Based on Sealed Water Calorimetry

Because the dose rate at the standard 1 m position from the ^{60}Co source was too low to achieve adequate precision, the calorimeter was positioned approximately 70 cm from the source, and the field size was adjusted to be 10 cm by 10 cm at the measurement depth of 5 cm. A pointer system attached to the head of the ^{60}Co unit was used to accurately position the calorimeter.

Figure 18 summarizes all of the ^{60}Co absorbed dose results obtained using the SW water calorimeter. This figure includes the data presented in figure 17 as well as several additional measurement sets. All of the correction factors, including that for the heat defect, have been applied. As pointed out in section 5, there appears to be a problem with our current estimate of the heat defect of the H_2/O_2 system at 4°C. In addition, we note that the 22°C results are systematically higher than the 4°C results. Work underway suggests that this discrepancy is due to convective heat transfer at 22°C, so we do not include the 22°C results in estimating the absorbed dose rate. Using all of the other data in figure 18 and referencing the dose rate to October 1, 1996 gives

$$\dot{D}_{\mathrm{w,SW}} = 1.610 \pm 0.57\% \ \ \mathrm{Gy/min.} \tag{12}$$

Leaving out the H_2/O_2 data reduces the dose by about 0.15%. The overall uncertainty ($1\ \sigma$) includes uncertainties on the heat loss correction factors (0.03%), positioning (0.14%),

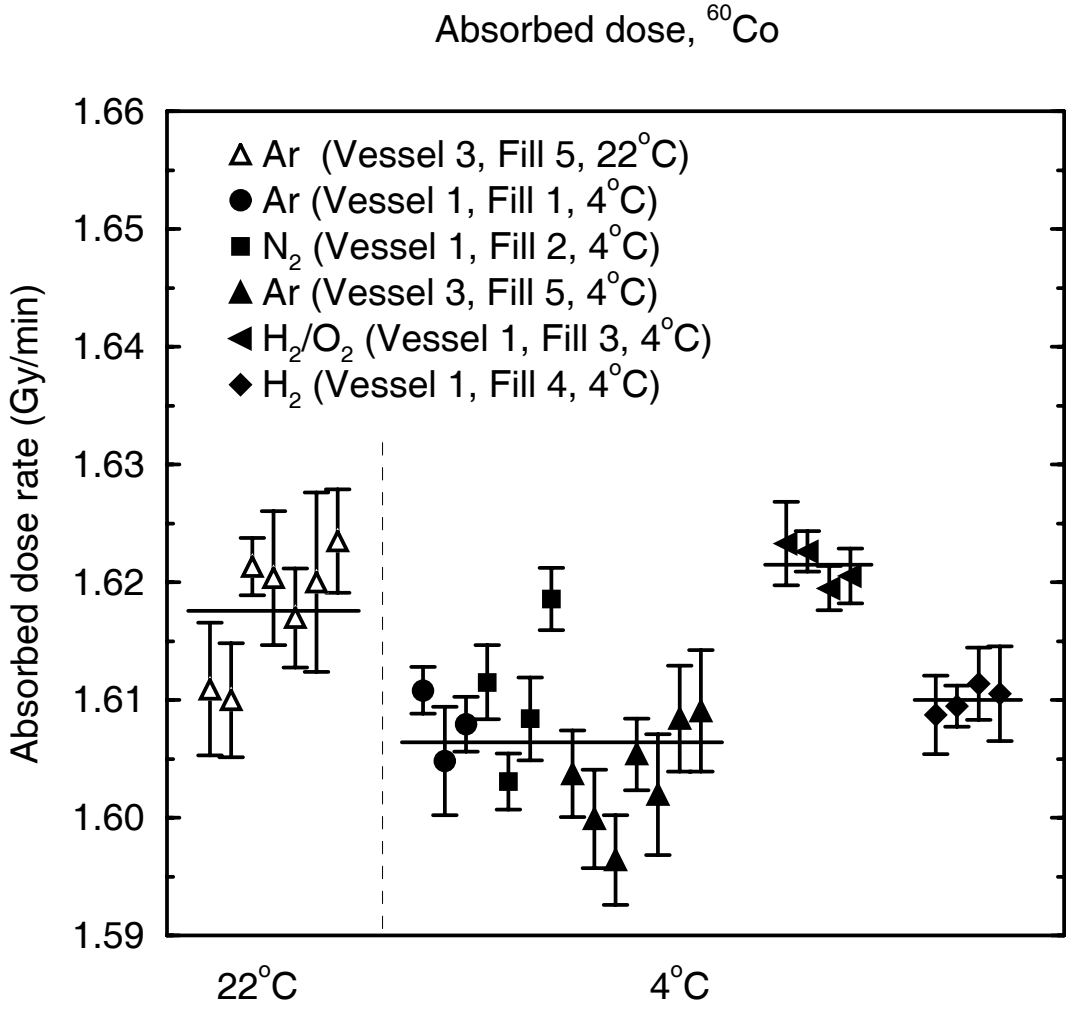

Figure 18: Summary of absorbed dose measurements for ^{60}Co obtained using the sealed water calorimeter. Each datum point is the mean of several calorimeter runs, and the statistical uncertainty on the mean is shown by the error bars. The horizontal lines represent the mean values of the data within each cluster.

field perturbation correction (0.05%), thermistor calibration constant (0.2%) and heat defect (0.5%).

Once the dose was established calorimetrically, the glass vessel was removed from the calorimeter phantom, and Fricke dosimeters were irradiated at the reference position. The ferrous sulfate solution was held in pillbox-shaped vials with either quartz or Lucite walls. The centre of each vial was positioned at a depth of 5 g/cm^2 and the vials were irradiated to nominal doses of 8, 12, 16 and 20 Gy. The absorbed dose, $D_{\mathrm{w,F}}$, can be determined from the measured change in optical density, ΔOD, using

$$D_{\mathrm{w,F}} = \frac{\Delta OD}{\rho l \epsilon G} f k_{\mathrm{vial}} k_{\mathrm{dd}}, \tag{13}$$

where ρ is the density of the ferrous sulfate solution (1.023 g cm^{-3}), l is the optical pathlength through the solution, ϵ is the extinction coefficient of the ferric ion, Fe^{3+}, and G is its radiation-induced chemical yield. The factor, f, converts the dose-to-Fricke to dose-to-water, k_{vial} corrects for the effect of the vial wall and k_{dd} accounts for transverse dose gradients over the vial. Values of f and k_{vial} were taken from Ma *et al* (1993), while k_{dd} was obtained from measured dose distributions (section 3.6). The results are summarized in table 4.

Radiation	k_{vial}		f	k_{dd}	depth
Quality	Lucite	quartz			(cm)
^{60}Co	0.9990	1.0001	1.0032	1.0021	5
20 MV	1.0011	0.9859	1.0023	1.0022	10

Table 4: Conversion factors and correction factors used in conjunction with the Fricke dosimeter vials for ^{60}Co γ-rays and 20 MV x-rays ($\mathrm{TPR}_{10}^{20} = 0.758$). The values of f and k_{vial} are from Ma *et al* (1993), while k_{dd} was measured for the present work. The uncertainties quoted on the calculated values of f and k_{vial} are about 0.05%, while those on k_{dd} are small enough to ignore.

In a typical experiment, 8 to 10 vials were irradiated and two to four vials were kept as controls. The precision obtained using the quartz vials was generally much better than that obtained using the plastic vials, but the measurements with both vial materials confirmed that the vial wall correction factor is close to unity for ^{60}Co.

The determination of $D_{w,F}$ using equation 13 requires knowledge of ϵG. Alternatively, we can substitute the dose determined calorimetrically, $D_{w,SW}$, for $D_{w,F}$ and solve equation 13 for ϵG. Doing so gives

$$\epsilon G(\mathrm{SW},\ ^{60}\mathrm{Co}) = 3.498 \pm 0.022 \quad \mathrm{cm}^2/\mathrm{J}. \tag{14}$$

6.2 Dose Based on Stirred Water Calorimetry

The Fricke calibration factor, ϵG, has also been determined using stirred water calorimetry (Ross *et al* 1989; Klassen *et al* 1991). From measurements using 20 MV x-rays the result is

$$\epsilon G(\mathrm{AW},\ 20MV) = 3.505 \pm 0.021 \quad \mathrm{cm}^2/\mathrm{J}, \tag{15}$$

where the label "AW" has been used to indicate "agitated water".

More recently, the stirred water calorimeter was used to establish the dose at ^{60}Co and calibrate Fricke solution at this radiation quality. These measurements led to a value for ϵG of (Ross *et al* 1994; Klassen *et al* 1999)

$$\epsilon G(\mathrm{AW},\ ^{60}\mathrm{Co}) = 3.474 \pm 0.019 \quad \mathrm{cm}^2/\mathrm{J}. \tag{16}$$

This result is 0.7% lower than that obtained using the sealed water calorimeter (equation 14) and 0.9% lower than the value at 20 MV.

Rather than expressing the relationship between the two calorimeters in terms of ϵG, the Fricke results can be used to compare the absorbed dose values that the two calorimeters would give. The result is

$$D_{w,SW}/D_{w,AW} = 0.993 \pm 0.008. \tag{17}$$

The uncertainty presented in equation 17 includes 0.5% for k_{HD}. Because the ratio of absorbed dose obtained using different water calorimeters is being reported, it might be expected that the correction for the heat defect cancels out. However, the results obtained with the stirred water calorimeter are based mainly on the H_2/O_2 aqueous system, while those obtained using the sealed water calorimeter are based mainly on hypoxic water. Figure 17 shows that our present model for the radiolysis of water leads to a significant discrepancy between these two systems, and this should be reflected in the uncertainty estimates.

6.3 Dose Based on Graphite Calorimetry

The NRC ^{60}Co source has also been calibrated in terms of absorbed dose to water using a graphite calorimeter (Henry 1977). This calibration is maintained using ion chambers and Fricke dosimetry and, until recently, constituted the Canadian absorbed dose to water standard at ^{60}Co. We calibrated a typical thimble chamber (model NE2571, s/n 667) against the Henry standard and used it to determine the dose to water at the reference point in the SW calorimeter. Comparing the dose established this way to that obtained using the SW calorimeter gives

$$D_{\mathrm{w,SW}}/D_{\mathrm{w,gr}} = 1.0093 \pm 0.008. \tag{18}$$

We note that if the gap correction of 0.37% were applied to the Henry calorimeter (Shortt *et al* 1993) this ratio would become 1.0056.

Figure 19 summarizes the present status of our data relating to the measurement of absorbed dose for ^{60}Co γ-rays. The value based on the NIST standard was obtained from a recent intercomparison using ion chambers[2]. The results indicate that the absorbed dose measured with the Henry calorimeter is low by 0.9 to 1.6%.

On 1 July, 1998, NRC declared that the sealed water calorimeter operating at 4°C will be the basis of its ^{60}Co standard for absorbed dose to water. Values for absorbed dose obtained using this new standard will be larger than the old Henry standard by about 0.9%.

7 20 MV Results

The 20 MV x-ray beam was produced by allowing 20 MeV electrons from the NRC accelerator to impinge on an aluminum target, 4.5 cm thick. A flat x-ray field was generated by sweeping the electron beam as described by Ross *et al* (1993) and no flattening filter was required. The beam was collimated using a Therac-20 collimator to a field size of 10 cm by 10 cm at the measuring depth of 10 cm. The beam quality indices, TPR^{20}_{10} and $\%\mathrm{dd}(10)_{\mathrm{x}}$, were measured to be 0.758 and 79.4, respectively.

[2]Private communication from one of the authors (Ken Shortt). Ken used a series of ion chambers to compare the NRC and NIST standards in 1998.

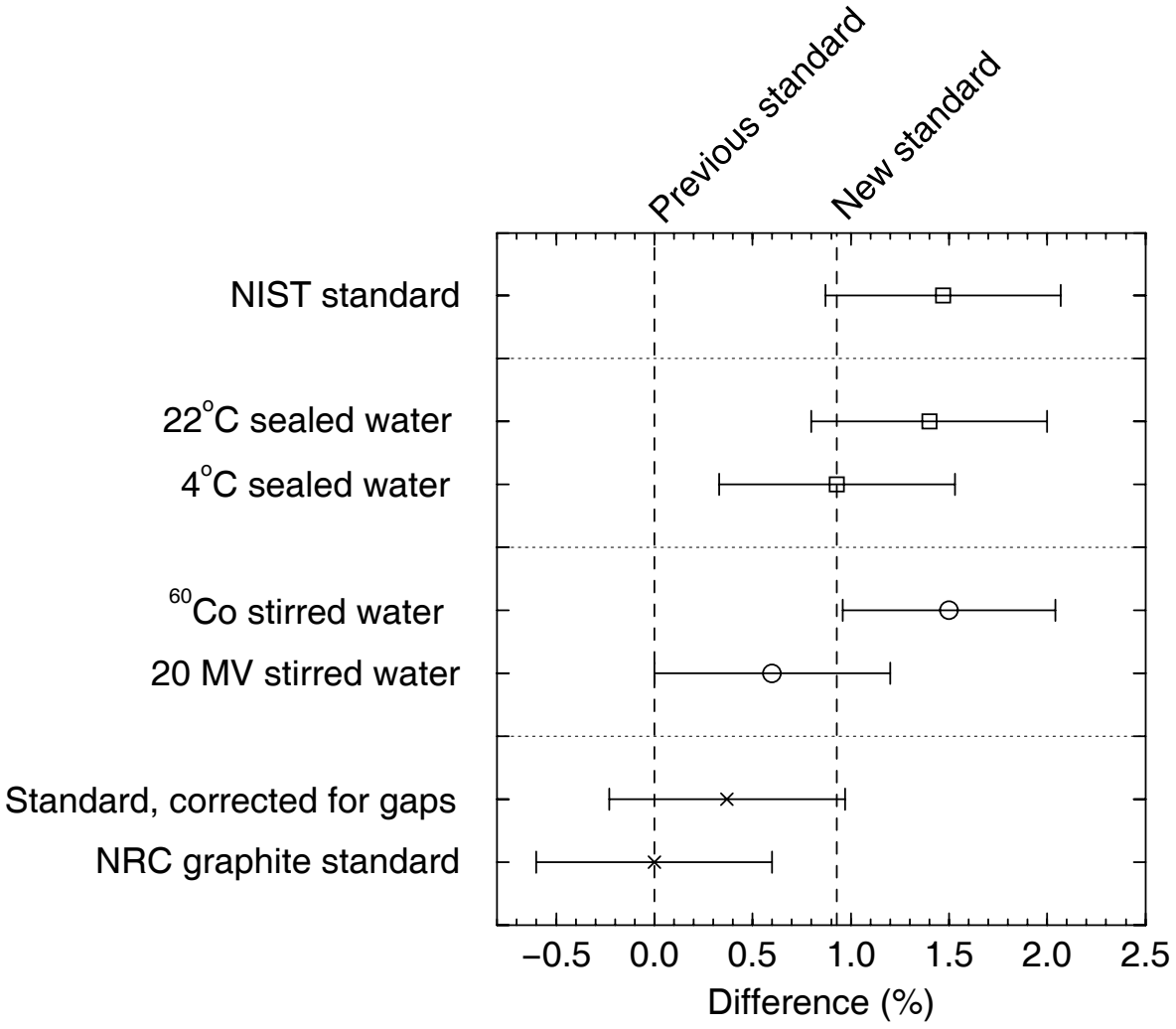

Figure 19: Summary of absorbed dose measurements for ^{60}Co obtained using various techniques. Differences are expressed as a percentage with respect to the original NRC standard for absorbed dose, which was based on the Henry graphite calorimeter. Three of the NRC results are no longer considered relevant: "NRC graphite standard" because no gap correction was applied; "20 MV stirred water" because of the variation of ϵG with energy; and "22°C sealed water" because of convective effects.

The calorimeter was positioned so that the entrance window on the Lucite tank was approximately 1 m from the upstream side of the target, and the dose rate at the measuring position was approximately 1.6 Gy/min. The x-ray beam was monitored using two transmission monitor chambers, one situated on the upstream side of the collimator and one on the downstream side. Day-to-day variations in the monitor chambers were tracked using a thimble chamber mounted in an aluminum block thick enough to provide full buildup. This assembly was placed in the beam just upstream of the calorimeter at least once a day and the thimble chamber output used to normalize the readings from the monitor chambers. The day-to-day changes in the monitor chambers was generally less than 0.4%.

All of the calorimeter measurements were done using vessel #3, and measurements were carried out at 22°C and 4°C. Once a series of measurements was completed, an NE2571 thimble chamber (s/n 667) was placed at the measurement point and its calibration factor determined. The ion chamber response was corrected for pressure and temperature, but no other corrections were applied. The results are summarized in figure 20, and the following features are evident:

- For the pure water system, the absorbed dose measured at 22°C is about 0.6% bigger than at 4°C.
- The H_2 system gives a value for the dose which agrees well with that obtained using the pure water system.
- At 22°C, the dose obtained using the H_2/O_2 system may be slightly larger ($\approx$0.2%) than that measured using the pure water system.
- At 4°C, the dose obtained using the H_2/O_2 system is significantly larger ($\approx$0.7%) than that measured using the pure water system.

Both the discrepancy with the H_2/O_2 system and the difference between 22°C and 4°C are consistent with the ^{60}Co results.

Fricke dosimeters were also irradiated at the reference point in the calorimeter phantom. The same procedure was used as for the ^{60}Co irradiations, and the various factors required in equation 13 are given in table 4. The value obtained for ϵG for 20 MV x-rays is given in

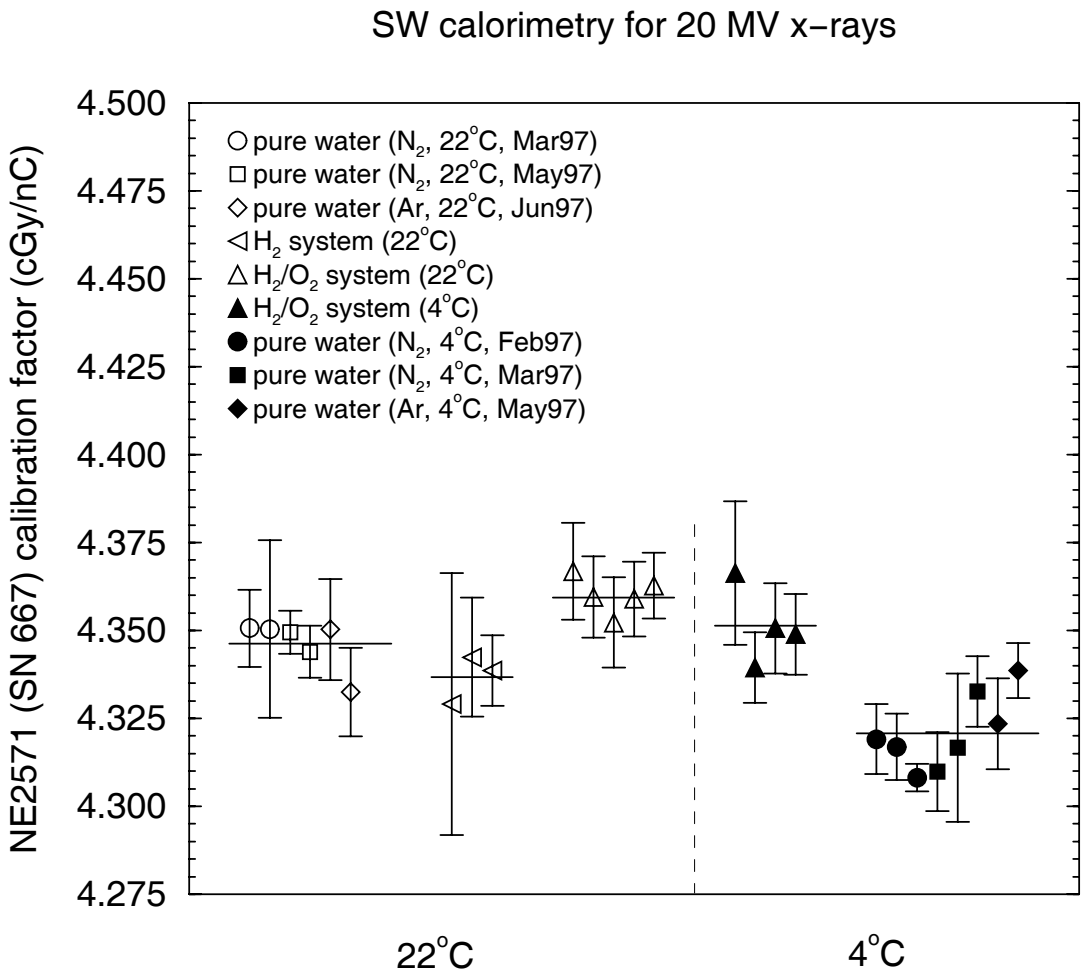

Figure 20: Summary of absorbed dose measurements for 20 MV x-rays obtained using the sealed water calorimeter. The results are given as the calibration factor (absorbed dose to water) obtained for a thimble ion chamber. (The ion chamber response was corrected for pressure and temperature, but no other corrections were applied). Each datum point is the mean of several calorimeter runs, and the statistical uncertainty on the mean is shown by the error bars. The horizontal lines represent the mean values of the data within each cluster.

table 5, along with the ^{60}Co result. Table 5 shows that the value of ϵG obtained with the

Radiation Quality	Number of independent experiments	ϵG (cm^2 J^{-1})
^{60}Co	5	3.499 ($\pm$ 0.60%)
20 MV(TPR$^{20}_{10}$ = 0.758)	4	3.521 ($\pm$ 0.65%)
Change in ϵG between 20 MV and ^{60}Co		0.63% ($\pm$ 0.53%)

Table 5: Values of ϵG for the Fricke dosimeter based on the NRC sealed water calorimeter operated at 4°C. The measured change in ϵG is shown in the last line. The uncertainties incorporate the systematic uncertainties associated with Fricke dosimetry and water calorimetry, including the 0.5% uncertainty on the heat defect. However, the uncertainty on the heat defect is not included in the uncertainty on the *change* of ϵG.

sealed water calorimeter increases by about 0.6% as the photon beam quality increases from ^{60}Co to 20 MV. This change is consistent with the change of 0.9% obtained with the stirred water calorimeter (section 6.2). All of our data on the variation of ϵG with beam quality is summarized and compared to the results obtained by others in a recent paper by Klassen *et al* (1999).

Equation 15 gives the value of ϵG obtained for 20 MV x-rays using the stirred water calorimeter, while the equivalent result for the sealed water calorimeter is given in table 5. These results can be used to compare the values of the absorbed dose to water for the two calorimeters, and the result is

$$D_{\mathrm{w,SW}}/D_{\mathrm{w,AW}} = 0.995 \pm 0.008. \tag{19}$$

Equations 17 and 19 show that the absorbed dose measured with the sealed water calorimeter is lower that that obtained using the stirred water calorimeter by 0.5 to 0.7%.

8 Discussion

Building on the work of others over the past twenty years, we have constructed a water calorimeter which will serve as the basis of the Canadian standard for absorbed dose to water for ^{60}Co γ-rays and high energy x-rays. Preliminary measurements and calculations indicate that it can also be used to establish the dose in electron beams with energies greater than 15 MeV. Some modifications to the sealed glass vessel may be necessary if the absorbed dose is to be measured for electron beams with energies below 15 MeV.

The main characteristics of the calorimeter can be summarized as follows:

- Separate glass vessel to control the water purity, and thus the heat defect, in the vicinity of the measuring point.
- Operation at any temperature from 0°C to 30°C.
- Designed for operation in horizontal beams.
- Computer-controlled operation.
- At clinical dose rates of about 1.5 Gy/min, the standard deviation is about 1%. Thus, a set of 10 runs leads to a standard uncertainty on the mean of about 0.3%. The precision improves as the dose rate increases.

Radiation-induced chemical reactions are thought to be the most likely mechanism giving rise to a heat defect in water calorimetry (Ross *et al* 1989). However, we continue to consider other mechanisms which might contribute to a heat defect, or which might affect the response of the calorimeter. The following have been examined during the course of this work:

- The effects of pressure on the specific heat of water. The glass vessel is filled and sealed at room temperature, but may be operated at 4°C. The volume occupied by the water decreases as the temperature decreases, but the size of the glass vessel changes very little, leaving the water under slight negative pressure.
- The effect of the flow of charge set in motion as a result of the radiation. High energy beams tend to transport charge along the beam axis and this charge must eventually flow back upstream.

- The radiation beam carries momentum into the water phantom which might lead to water movement along the beam axis.

Rough estimates indicate that none of these mechanisms will have a measurable impact on the calorimeter response.

The results of absorbed dose measurements at ^{60}Co and 20 MV are summarized in table 6. All known corrections, except for the heat defect, have been applied. The main results can be summarized as follows:

- Type A standard uncertainties of 0.2% or better are achievable. The largest type B uncertainty is due to the heat defect and is about 0.5%.

- The measurements are consistent with a heat defect of 2.4% for the H_2/O_2 system at both 4 and 22°C. Calculations based on Model III predict only 1.6% at 4°C. The reason for this discrepancy is under investigation.

- The calorimeter response at 22°C is about 0.6% greater than at 4°C. This is now understood to be due to convective heat transfer at 22°C, and a paper on this work is in preparation.

^{60}Co							
System	No. of sets	No. of runs	Apparent Dose Rate (Gy/min)		Ratio to pure		Ratio
			22°C	4°C	22°C	4°C	22°C/4°C
pure	7/14	106/191	1.617 (± 0.12%)	1.606 (± 0.10%)	1.0000	1.0000	1.0068
H_2/O_2	-/4	-/30	-	1.648 (± 0.07%)	-	1.0262	-
hydrogen	-/4	-/69	-	1.611 (± 0.10%)	-	1.0031	-

20 MV							
System	No. of sets	No. of runs	Apparent $N_{D,w}$ (NE2571, s/n 667)		Ratio to pure		Ratio
			22°C	4°C	22°C	4°C	22°C/4°C
pure	6/8	104/96	4.346 (± 0.13%)	4.323 (± 0.10%)	1.0000	1.0000	1.0053
H_2/O_2	5/4	81/36	4.449 (± 0.14%)	4.421 (± 0.16%)	1.0237	1.0227	1.0063
hydrogen	3/-	40/-	4.337 (± 0.26%)	-	0.9979	-	-

Table 6: Results of SW calorimeter measurements using ^{60}Co γ-rays and 20 MV x-rays. Measurements were carried out at 4°C and 22°C using three aqueous systems. In columns 2 and 3, the number before the slash refers to 22°C and the number after to 4°C. The number of individual irradiations contributing to each result is given in column 3. A set (column 2) represents ten or more individual runs which have been averaged to produce a single datum in figures 18 and 20. The ^{60}Co results are reported as a dose rate, while the 20 MV results are expressed as the calibration factor (corrected for only pressure and temperature) for a NE2571 thimble chamber. The adjective "apparent" is used because no heat defect correction has been applied. Only the statistical uncertainties are listed in columns 4 and 5.

9 Acknowledgements

The knowledge, skill and dedication of NRC's technical and support staff were critical for the successful outcome of this work. The glass cylinders which form the central portion of the sealed glass vessels were ground by Gary Boyd. The rest of the glass work, including the glass envelopes for the thermistor probes, was done by Peter l'Abbé. David Marchington was responsible for the overall assembly of the calorimeter and he also constructed the internal bead and lead assemblies for the thermistor probes. Leo Heistek constructed the bridge circuit and the electronics for automated control. The original software for reading and analysing the data from the calorimeter was converted into Windows-based applications by a summer student, Dylan Togane.

Other members of the IRS Group have provided advice and criticism as appropriate. Iwan Kawrakow was prepared to tackle the problem of modelling convective flow and this has led to new insights as to how convection can affect calorimeter response. Dave Rogers read the final manuscript and provided many useful comments.

References

Chauvenet B, Baltès D and Delaunay F 1997 Comparison of graphite-to-water absorbed-dose transfers for ^{60}Co photon beams using ionometry and Fricke dosimetry *Phys. Med. Biol.* **42** 2053–2063

Domen S R 1980 Absorbed dose water calorimeter *Med. Phys.* **7** 157–159

Domen S R 1982 An absorbed dose water calorimeter: Theory, design and performance *J. Res. NBS* **87** 211–235

Domen S R 1987 Advances in calorimetry for radiation dosimetry In *The Dosimetry of Ionizing Radiation, Vol. II*, K. R. Kase, B. E. Bjarngard, and F. H. Attix (Eds.), pp. 245–320 Academic Press: Orlando

Domen S R 1988 Convective velocity effects on a thermistor in water *J. Res. NBS* **93** 603–612

Domen S R 1994 A sealed water calorimeter for measuring absorbed dose *J. Res. Natl. Inst. Stand. Tech.* **99** 121–141

DuSautoy A R 1996 The UK primary standard calorimeter for photon-beam absorbed dose measurement *Phys. Med. Biol.* **41** 137–15

Elliot A J 1994 Rate constants and G-values for the simulation of the radiolysis of light water over the range 0–300°C Technical Report AECL-11073, Atomic Energy of Canada Ltd., Chalk River, Canada

Guerra A S, Laitano R F and Pimpinella M 1996 Characteristics of the absorbed dose to water standard at ENEA *Phys. Med. Biol.* **41** 657–674

Henry W H 1977 The NRC absorbed dose to water calibration service NRC Flyer, National Research Council, Ottawa, Canada

Klassen N V and Ross C K 1991 Absorbed dose calorimetry using various aqueous solutions *Radiat. Phys. Chem.* **38** 95–104

Klassen N V and Ross C K 1997 Water calorimetry: The heat defect *J. Res. Natl. Inst. Stand. Technol.* **102** 63–74

Klassen N V, Shortt K R and Ross C K 1991 Calibration of Fricke dosimetry by water calorimetry In *Proc. 7th Tihany Symp. Rad. Chem.*, Budapest, pp. 543–547 Hungarian Chemistry Soc.

Klassen N V, Shortt K R, Seuntjens J and Ross C K 1999 Fricke dosimetry: The difference between G(Fe^{3+}) for ^{60}Co γ-rays and high energy x-rays *Phys. Med. Biol.* (submitted)

Laughlin J S and Genna S 1966 Calorimetry In *Radiation Dosimetry, Vol. II*, F. H. Attix and W. C. Roesch (Eds.), pp. 389–441 Academic Press: New York

Ma C M, Rogers D W O, Shortt K R, Ross C K, Nahum A E and Bielajew A F 1993 Wall correction and absorbed dose conversion factors for Fricke dosimetry: Monte Carlo calculations and measurements *Med. Phys.* **20** 283–292

Palmans H, Seuntjens J, Verhaegan F, Denis J M and Vynckier S 1996 Water calorimetry and ionization chamber dosimetry in an 85-MeV clinical proton beam *Med. Phys.* **23** 643–650

Roos M 1988 The current status of water absorbed dose calorimetry in the PTB In *NRC Workshop on Water Calorimetry*, C. K. Ross and N. V. Klassen (Eds.), Ottawa, Canada, pp. 9–15 National Research Council

Ross C K and Klassen N V 1996 Water calorimetry for radiation dosimetry *Phys. Med. Biol.* **41** 1–29

Ross C K, Klassen N V and Shortt K R 1994 The development of a standard based on water calorimetry for absorbed dose to water In *NPL Calorimetry Workshop*, Teddington, UK National Physical Laboratory

Ross C K, Klassen N V, Shortt K R and Smith G D 1989 A direct comparison of water calorimetry and Fricke dosimetry *Phys. Med. Biol.* **34** 23–42

Ross C K, Klassen N V and Smith G D 1984 The effect of various dissolved gases on the heat defect of water *Med. Phys.* **11** 653–658

Ross C K, Shortt K R, Rogers D W O and Delaunay F 1993 A test of TPR^{20}_{10} as a beam quality specifier for high energy photon beams In *Proc. Symp. on Measurement Assurance in Dosimetry IAEA-SM-330/10*, (Vienna: IAEA) 309–321

Schulz R J, Huq M S, Venkataramanan N and Motakabbir K A 1991 A comparison of ionization-chamber and water-calorimeter dosimetry for high-energy x-rays *Med. Phys.* **18** 1229–1233

Schulz R J and Weinhous M S 1985 Convection currents in a water calorimeter *Phys. Med. Biol.* **30** 1093–1099

Schulz R J, Wuu C S and Weinhous M S 1987 The direct determination of dose-to-water using a water calorimeter *Med. Phys.* **14** 790–796

Seuntjens J 1991 *Comparative Study of Ion Chamber Dosimetry and Water Calorimetry in Medium Energy X-Ray Beams* Ph. D. thesis, Gent University, Gent, Belgium

Seuntjens J and Palmans H 1999 Correction factors and performance of a 4°C sealed water calorimeter *Phys. Med. Biol.* **44** 627–646

Seuntjens J, Thierens H and Schneider U 1993a Correction factors for a cylindrical ionization chamber used in medium energy x-ray beams *Phys. Med. Biol.* **38** 805–832

Seuntjens J, Van der Plaetsen A, Van Laere K and Thierens H 1993b Study of the relative heat defect and correction factors of a water calorimetric determination of absorbed dose to water in high-energy photon beams In *Proc. Symp. on Measurement Assurance in Dosimetry IAEA-SM-330/6*, (Vienna: IAEA) 45–59

Shortt K R, Ross C K, Schneider M, Hohfeld K, Roos M and Perroche A M 1993 A comparison of absorbed dose standards for high-energy x-rays *Phys. Med. Biol.* **38** 1937–1955